Contributions to Mineralogy and Petrology (2024) 179:16
https://doi.org/10.1007/s00410-023-02091-z

ORIGINAL PAPER

Rapid accumulation and ascent precedes caldera forming eruption of low viscosity magma

Corin Jorgenson[1] · Luca Caricchi[1] · Massimo Chiaradia[1] · Mónica Ágreda-López[2] · Guido Giordano[3]

Received: 29 June 2023 / Accepted: 15 December 2023 / Published online: 1 February 2024

Abstract

Mafic magma is commonly associated with effusive eruptions, however several mafic volcanoes throughout the globe have produced explosive eruptions. Here we present one such volcano – Colli Albani. Colli Albani is 20 km SE of Rome and produced seven large volume ignimbrites. Field observations, mineral chemistry, and Sr and Nd isotopes in clinopyroxene show that the high potassic, silica undersaturated and CO_2-rich magma typical of Colli Albani is produced by partial melting of a metasomatized mantle. Clinopyroxene based thermobarometry combined with thermal modelling, indicates rapid accumulation of magma into the shallow crust preceding the last caldera forming event (355 ka). The crystallization of high Mg# and high Cr_2O_3 clinopyroxenes at low pressures and high temperatures indicates rapid magma ascent from the mantle. We suggest that a final rapid input of this deeply sourced magma destabilised the shallow and fast assembled magma reservoir and lead to the caldera forming event. Our findings have significant implications for the evaluation of the timescales of reactivation of Colli Albani and other similar long-quiescent calderas erupting low viscosity magmas, as rapid migration of magma to shallow reservoirs may result in short unrest periods prior to a large eruption.

Keywords Alkaline volcanism · Rapid ascent · Sustained mafic eruption · Colli Albani

Introduction

Colli Albani (CA) is a volcano in central Italy, 20 km SE from the ~3 million people living in Rome (Fig. 1a). CA erupts magma that is both mafic and alkaline. CA is part of the Roman Magmatic Province, which is a Quaternary chain of K-alkaline calderas and stratovolcanoes. The Roman Magmatic Province is associated with the complex and fast geodynamic evolution of central Italy during the Cenozoic, involving subduction of continental crust followed by back-arc extension (Conticelli et al. 2010; Giordano and Caricchi 2022). CA produced seven sustained caldera forming eruptions (Volcanic explosivity index - VEI 6-7) during its eruptive history, which started 600 ka (Giordano 2010). This is surprising given that mafic-alkaline magmas commonly erupt effusively due to the low silica and high alkali content resulting in a very low viscosity. Such low viscosity favours outgassing of exsolved volatiles thus decreasing the eruptive potential to erupt explosively (Cassidy et al. 2018; Giordano et al. 2008). There are several known examples of basaltic explosive eruptions (Fontana Lapilli, Masaya Triple Layer, Etna 122 BC, Tarawera 1886) however the difference in viscosity between a mafic and a mafic-alkaline melt like CA has several consequences in terms of bubble coalescence and growth, bubble rise speeds, and volatile solubility (Costantini et al. 2009; Hlinka et al. 2021; Giordano and Dingwell 2003; Rowe et al. 2021; Ohashi et al. 2022; Vetere et al. 2014; Huber et al. 2014; Sable et al. 2006). The CA caldera complex is even more anomalous with respect to basaltic volcanoes because of the high content of K_2O, which further lowers magma viscosity to vary between 10^2 and 10^6 Pa s, temperature and volatile dependent (Campagnola et al. 2016; Giordano et al. 2008; Vinkler et al. 2012). Although CA has not erupted in over

Communicated by Dante Canil.

✉ Corin Jorgenson
corin.jorgenson@unige.ch

[1] Department of Earth Science, University of Geneva, Rue de Maraîchers, 13, 1205 Geneva, Switzerland

[2] Department of Physics and Geology, University of Perugia, Via Alessandro Pascoli, 06123 Perugia, Italy

[3] Department of Science Geology, University of Roma Tre, 446 Viale Guglielmo Marconi, 00146 Rome, Italy

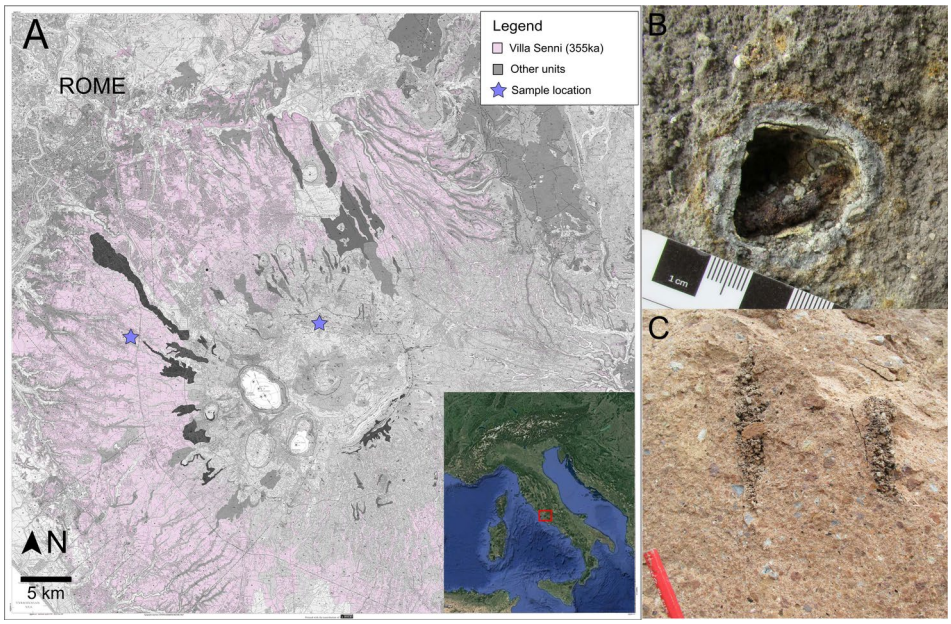

Fig. 1 **a** Geologic map of the Colli Albani region, modified from (Giordano 2010) with a regional inset modified from Google Earth. The purple stars show sample locations and where images **b** and **c** were taken. **b** Carbonate clast which has reacted to form delicate pyroxene dendrites in situ. **c** Degassing pipes seen at the Imater quarry within the RED unit

23 ka, it still exhibits sustained CO_2 degassing (>4.2x10^9 mol $year^{-1}$) and uplift over the last 70 years (Trasatti et al. 2018; Chiodini et al. 2004; Giordano 2010; Chiarabba et al. 1997). We can compare CA to other volcanoes using a compilation of volcanoes from Giordano and Caricchi (2022) in Fig. 2. This comparison shows that CA produces anomalously large eruptions for magma of its composition (Fig. 2). Furthermore, CA has a Volcanic Activity Index normalized (VAIn, a normalized value of the log of the ratio between the DRE and the age of the last eruption times average eruption rate) of 0.48, which is higher than the VAIn of Yellowstone (0.32) and InSar deformation and teleseismic data confirm the presence of magma at depth (Trasatti et al. 2018; Bianchi et al. 2008). Thus CA is an excellent case study to unveil the causes of such large and intense eruptions of low viscosity magma.

Carbonate assimilation results in the addition of excess CO_2 to the magma, which decreases its density and therefore either increases the pressure within a magma reservoir or, if the assimilation occurs during ascent (Aiuppa et al. 2021; Knuever et al. 2022), will lead to acceleration toward the surface favouring the generation of overpressure and fragmentation (Gonnermann and Manga 2007). Several authors propose that assimilation of shallow Meso-Cenozoic carbonates, which are present beneath the CA at depths between 1 and 5 km, is ultimately the

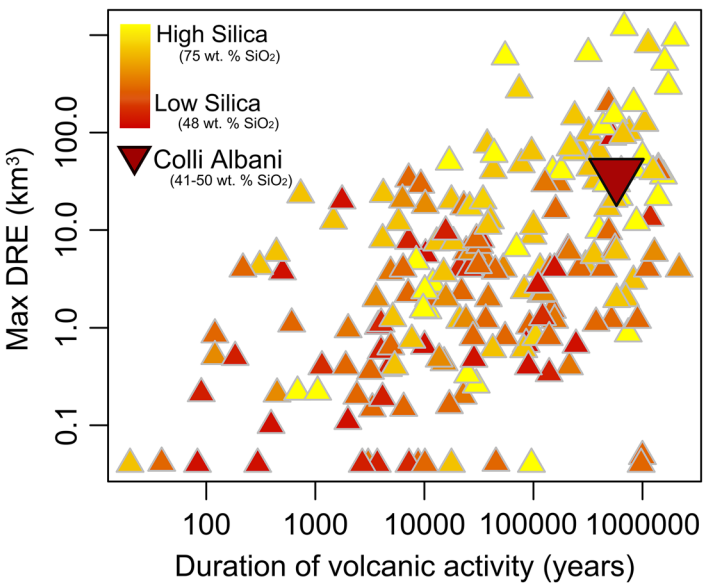

Fig. 2 Volume of largest eruption versus total duration of volcanic activity for volcanoes worldwide, colour contoured for the end members of silica content (48–75 wt.% SiO_2 and adapted after Giordano and Caricchi 2022). Colli Albani falls into a region with a large max DRE and long duration, however is somewhat anomalous in the compositional space. Figure adapted from Higgins and Caricchi (2023)

cause behind the anomalous behaviour of this volcanic system (Freda et al. 2011; Bianchi et al. 2008; Iacono-Marziano et al. 2007; Mollo et al. 2010; Cross et al. 2014; Conticelli et al. 2010; Dallai et al. 2004). Support for the shallow carbonate assimilation hypothesis comes from experimental work of Iacono-Marziano et al. (2007) who suggests 0–15 wt.% of assimilation is needed to follow the abnormal liquid line of descent for CA magma, which is controlled by the crystallization of clinopyroxene and leucite and does not evolve to higher silica (Gaeta et al. 2006). Additionally, geophysical evidence shows the present magmatic reservoir is partially emplaced within Mesozoic carbonate sediments at ~5 km depth (Freda et al. 2011; Bianchi et al. 2008; Iacono-Marziano et al. 2007; Mollo et al. 2010). Other studies instead argue that carbonate metasomatism in the mantle contributes to generate the anomalous chemistry of magma erupted at CA as well as to the very high CO_2 flux in the whole central Italy (Conticelli et al. 2010; Gaeta et al. 2006; Dallai et al. 2004; Boari et al. 2009; Chiodini et al. 2004; Avanzinelli et al. 2018).

Several experimental studies have shown that decarbonation is a rapid process occurring on the scale of seconds to hours (Freda et al. 2011; Knuever et al. 2022; Blythe et al. 2015). On the other hand, geochemical characteristics and evolution are long-term processes happening on the scale of years to thousands of years or more depending on the volumes involved (Gaeta et al. 2006). When considering the processes responsible for the explosivity of eruptions at CA, it is important to consider that the deposits suggest that the eruption was sustained (e.g. absence of banding in the deposits; Giordano and Cas 2021), which requires full coupling between excess volatile phase and magma (Gonnermann and Manga 2007; Sparks 2003). Experimental investigations of the viscosity, bubble and microlite textures, viscosity calculations, and juvenile spatter all indicate that the magma erupted during these caldera forming events at Colli Albani were of low viscosity at the time of fragmentation (Vinkler et al. 2012; Campagnola et al. 2016). As the tendency for the excess volatile phase to decouple from magma increases with decreasing magma viscosity, gas-magma coupling in low viscosity magma can only occur if the velocity of magma ascent is elevated. Here we focus on the last caldera forming eruption of CA and use evidence from the field, petrography, mineral chemistry, and geochemistry collected on the products of the last large volume eruption of CA to identify the processes responsible for the sustained and explosive nature of eruptions at Colli Albani.

Stratigraphy

The last three large volume ignimbrites Pozzolane Rosse (RED, 457±4 ka, 37 km^3 dense rock equivalent, DRE, outflow and 26 km^3 DRE intracaldera), Pozzolane Nere (PNR, 404±4 ka, 10 km^3 DRE outflow and 5 km^3 DRE intracaldera), and Villa Senni (VSN, 351–357±3 ka, 18 km^3 DRE outflow and 10 km^3 DRE intracaldera) at CA make up the largest part of the Vulcano Laziale Edifice and are the best exposed of all the large volume ignimbrites (Giordano 2010; Karner et al. 2001). Carbonate lithics in these units have been used as evidence for carbonate assimilation in the upper crust, as they indicate that part of the plumbing system is established within carbonate host rocks (Freda et al. 2011). However, the concentration of carbonate clasts throughout the three units is variable, with VSN and PNR having significantly fewer carbonate clasts compared to RED - yet with comparable eruptive style and erupted volume (Giordano 2010).

Here we focus on VSN as it is the last and best exposed of the CA ignimbrites and as it has a similar eruption sequence, VEI, lithic abundance, and chemistry so can provide an analogue for all the CA ignimbrites (Fig. 1a pink unit). The eruption occurred at 355 ka, and produced a 18 km^3 DRE ignimbrite extending into the city of Rome (Karner et al. 2001; Diano et al. 2010). The formation is comprised of a basal fallout (VSN0) and two ignimbrites: Tufo Lionato Ignimbrite (VSN1) and Pozzolanelle Ignimbrite (VSN2), which are separated by a co-ignimbrite breccia at some localities (VSN2b; Vinkler et al. 2012). The basal unit (VSN0) usually consists of a plane parallel to faintly cross stratified, fine- to coarse-ash fall deposit, up to 1.3 m in proximal sections and extending eastward more than 20 km from the caldera (Giordano 2010). In some proximal locations, a few cm thick surge deposit with low angle cross laminations, which is fine grained and well sorted, is also present at the very base (Giordano 2010). This is overlain by the Tufo Lionato Ignimbrite (VSN1), named for the yellow to orange/red colour caused by zeolite alteration. In general, the deposit is massive, structureless, and exhibits reverse grading of scoria and lithic clasts (Vinkler et al. 2012). It is an ash rich, matrix supported deposit with most clasts consisting of aphyric scoriae with minor spatter clasts, lava lithics, and rare carbonate clasts. The Pozzolanelle Ignimbrite covers the same area as the Tufo Lionato and has an average thickness of 20 m and a maximum thickness of 80 m. The average composition of scoria ranges from tephritic to tephritic-phonolitic (Conticelli et al. 2010). It is a dark grey to dark red ignimbrite characterized by massive and chaotic facies throughout and generally is not zeolitized. It is matrix supported, consisting of coarse ash shards and crystal fragments. The framework is reddish to black aphyric to highly porphyritic scoria clasts. The top of the unit is locally conformably covered

by planar bedded scoria lapilli beds (fallout deposits from Plinian to sub Plinian plumes erupted post main eruption). Within the Pozzolanelle ignimbrite there are two lithofacies: VSN2, which is crystal rich with leucite and clinopyroxene present in the matrix and as phenocrysts and VSN2b, which is a breccia with lapilli to block sized (max 2 m) clasts, dominated by juveniles (60–90%), and up to 30% lava clasts, carbonate clasts, metamorphic clasts, and intrusive leucite-pyroxene cumulates. Ages for these units are 355 ± 2 ka and 357 ± 2 ka for Tufo Lionato and Pozzolanelle respectively, which gives the stratigraphically younger unit an older age, however within error (Giordano 2010; Karner et al. 2001). Much of the VSN unit is zeolitized, which makes bulk XRF on these units near impossible.

Methods

Samples and analysis

In situ bulk samples of VSN ignimbrites were sampled stratigraphically at several localities around the volcanic centre for each subunit. Samples of ignimbrite material were taken at locations with minimal alteration and juvenile clasts were preferentially selected. Bulk samples were crushed, sieved, and sorted for clinopyroxene. The major element (SiO_2, Na_2O, CaO, MnO, Al_2O_3, NiO, MgO, TiO_2, FeO, and Cr_2O_3) composition of clinopyroxene phenocrysts was determined with a JEOL 8200 superprobe EPMA housed at the University of Geneva, using a focused spot (0 µm) at 15 keV and 20 nA. We make the assumption that all FeO is ferrous, though we note that there is likely Fe_2O_3 in the system as well. We follow standard operating procedures and additionally measure a standard every 60–100 points to ensure quality data. Standards used can be found in the Supplementary data. Analyses were filtered on the basis of totals within 99.0% and 101.0% and cation totals between 3.92 and 4.08. Errors, calculated from the percent analytical sensitivity and applied to our data (MacDonald 2017), SiO_2 ± 0.07 wt.%, Na_2O ±0.01 wt.%, FeO ±0.03 wt.%, Al_2O_3 ± 0.02 wt.%, CaO ±0.03 wt.%, MgO ± 0.05 wt.%, TiO_2 ± 0.01 wt.% and < 0 wt.% for MnO, NiO, Cr_2O_3. We collected back scattered electron (BSE) images and point transects from 121 clinopyroxenes (VSN0 $n = 26$, VSN1 $n = 37$, VSN2b $n = 30$, VSN2 $n = 28$) and single point analysis on 120 crystals, resulting in 2387 analyses of major phases. Geochemical results are visualized in Fig. 4 and accessible in Supplementary Data.

Isotopic measurements and modelling

Clinopyroxene separates were first measured via EPMA then removed and cleaned of any epoxy via multiple baths of acetone and ultrasonicated in deionized water prior to isotopic measurements. Radiogenic isotope ratios of $^{87}Sr/^{86}Sr$ and $^{143}Nd/^{144}Nd$ of single crystals were measured at the University of Geneva, following the methodology of Chiaradia et al. (2020) and analysed using a Neptune Plus MC-ICPMS. Between 5 and 15 mg of clinopyroxene were dissolved in Savillex ® Teflon vials during 7 days in Savillex ®Teflon vials using 4 ml of concentrated HF and 1 ml of HNO_3 14 M, at a temperature of 140°C and with the help of ultrasonication for 30 min twice a day. Subsequently, samples were dried and re-dissolved in 3 ml of HNO_3 14 M and dried again. Sr and Nd were separated using cascade columns with Sr-Spec, TRU-Spec and Ln-Spec resins according to a protocol modified from Pin et al. (1994). Finally, the material was redissolved in 2% HNO_3 solutions and ratios were measured using a Thermo Neptune PLUS Multi-Collector ICP-MS in static mode. Ratios used to monitor internal fractionation were: $^{87}Sr/^{86}Sr = 8.375209$ for the $^{87}Sr/^{86}Sr$ ratio and $^{143}Nd/^{144}Nd = 0.7219$ for the $^{143}Nd/^{144}Nd$ ratio. Used external standards were SRM987 ($^{87}Sr/^{86}Sr = 0.710248$; McArthur et al. 2001; long-term external reproducibility based on ~650 analyses over several years: 17 ppm, 1SD) and JNdi-1 ($^{143}Nd/^{144}Nd = 0.512115$; Tanaka et al. 2000; long-term external reproducibility based on ~340 analyses over several years: 14 ppm, 1SD). $^{87}Sr/^{86}Sr$ and $^{143}Nd/^{144}Nd$ isotope ratios were further corrected for external fractionation (due to a systematic difference between measured and the above reported accepted standard ratios) by values of − 0.021 ‰and + 0.051 ‰amu, respectively. Interferences at masses 84 (^{84}Kr), 86 (^{86}Kr) and 87 (^{87}Rb) were corrected by monitoring ^{83}Kr and ^{85}Rb, ^{144}Sm interference on ^{144}Nd was monitored on the mass ^{147}Sm and corrected by using a $^{144}Sm/^{147}Sm$ value of 0.206700. Total procedural blanks were <100 pg for Sr and Nd, which are insignificant compared to the amounts o f these elements purified from the samples investigated.

We used the DePaolo (1981) model to test if mixing between a depleted mantle source and regional T uscan carbonates ($^{87}Sr/^{86}Sr$ 0.7078−0.7089, Fig. 7a), which can be used as a proxy for the CA basement carbonates (Fig. 7), can yield the VSN isotopic signatures (Conticelli et al. 2009; Stoppa and Rosatelli 2009; Battistini et al. 2001; Melluso et al. 2004; Gagnevin et al. 2004).

Thermobarometry

We use a machine learning approach to estimate the pressure and temperature of crystallization of clinopyroxene crystals. While there are classical regression based thermobarometers which are calibrated for mafic magmas (e.g. Putirka 2008; Wang et al. 2021; Neave and Putirka 2017) and one for alkaline magmas (e.g. Masotta et al. 2013) there are no classical clinopyroxene thermobarometers for both

mafic and alkaline magmas. Therefore, we turn to developments in thermobarometry via a machine learning technique called random forest which is better calibrated for mafic and alkaline magma than other existing models (Jorgenson et al. 2022; Petrelli et al. 2020). With this approach an algorithm is trained on a calibration data set comprised of >2000 experimentally generated clinopyroxenes and learns how to estimate the pressure (P) and temperature (T). We use the clinopyroxene-only "Plug and Play" model of Jorgenson et al. (2022), which is developed in the freeware program R and available online. Readers are directed there for further information on the theory and methodology. P and T estimates are calculated for single points on line transects of zoned clinopyroxene, thus estimates will vary according to the chemical variations for each zone. Estimates were filtered if the interquartile range was above 6.4 kbar, which results in a standard error estimate (SEE) of 3.2 kbar and 75.5 ° C. We note that while the precision of this approach is relatively low, the estimates are internally consistent and allow to distinguish between storage in restricted versus transcrustal regions in the crust. In the following we will show how this provides important constraints on the processes leading to the caldera forming Villa Senni eruption.

Thermal modelling

To estimate the maximum residence of magma in the upper crust, we perform 1D thermal modelling considering the results obtained from the thermobarometry. We consider a footprint of the magmatic system varying between the caldera structural radius of 4 km, and the radius of 10 km of the area which encloses most of the CA vents (Giordano 2010). With a DRE volume of 18 km^3 and assuming the entire chamber is evacuated during the caldera collapse, we use the footprint of the magmatic system to estimate the thickness of the magma body (360 and 60 m for a 4 and 10 km radius, respectively). Under these assumptions, we used the 1D analytical solution from Jaeger (1965):

$$T = T_w + \frac{T_m + T_w}{2}\left[erf\left(\frac{x-b}{2\sqrt{\kappa t}}\right) - erf\left(\frac{x+b}{2\sqrt{\kappa t}}\right)\right] \quad (1)$$

Where T_w is the temperature of the wall rock, T_m is the magma temperature (1473 K), x is the distance from the centre of the intrusion, b is the half thickness of the intrusion (in m), t is the time (in s), and κ is the thermal diffusivity (0.5e−6 m^2/s) (Whittington et al. 2009). To determine the maximum possible duration of magma storage in the upper crust, we consider that magma injection before the eruption occurred in a preexisting reservoir at an arguably high temperature of 800 ° C.

Results

Clinopyroxene textures

We collected line transects and BSE images from 122 clinopyroxene crystals (VSN0 n = 26, VSN1 n = 37, VSN2b n = 30, VSN2 n = 29). From the BSE images, we defined four main textural subgroups (Fig. 3), though we note some degree of overlap between the different groups: patchy, patchy-zoned, sector zoned and simple. (1) Patchy, as seen in BSE images (Fig. 3a) corresponds to textures that are non-continuous and indicate resorption, also called spongy or vermicular (Streck 2008; Tomiya and Takahashi 2005; Brehm and Lange 2020). Patchy textures can result from zoned crystals changing via intra-crystal diffusion or due to melt-crystal equilibrium of unzoned crystals (Streck 2008; Tomiya and Takahashi 2005). These crystals vary for all the subunits (VSN0 n = 10, VSN1 n = 10, VSN2b n = 16, VSN2 n = 7) and often host melt inclusions. Notably, this is overwhelmingly the dominant phase for VSN0. (2) Patchy-zoned crystals, in most cases represent a patchy core, which is often melt inclusion rich, and zoned rims (Fig. 3b). We have also included in this subgroup the reverse case where a homogeneous or a zoned core is associated with a patchy rim, of which we only have a couple crystals with this feature. Of this group there are no VSN0 crystals which belong to this group, while they are relatively evenly distributed in the VSN ignimbrite (VSN1 n = 4, VSN2b n = 9, VSN2 n = 10). (3) Sector zoned crystals have an hourglass sector {111}, enriched in Si and Mg, with respect to the prism (Fig. 3c; Neave et al. 2019; Ubide et al. 2019). In some cases a sector zoned core is surrounded by a zoned outer rim of crystal. This type of zoning is mostly seen in VSN1 (n = 6) and a single crystal in VSN2 (n = 1). We loosely define the {111} sector as the triangle shaped regions on the c-axis of the crystal, also described as an hourglass form (Ubide et al. 2019). Following Ubide et al. (2019) we refer to the portions of the crystal perpendicular to the {111} sector as the prism sector. 4) Simple texture do not show any zoning or have rarely a distinguishable rim (Fig. 3d). These crystals sometimes host melt inclusions or cavities (VSN0 n = 16, VSN1 n = 17, VSN2b n = 5, VSN2 n = 11).

Clinopyroxene geochemistry

Chemical variability by subunit

To gain a holistic view of the clinopyroxene variability we look at the major element compositions in the subunits and as function of the textures defined in the previous section.

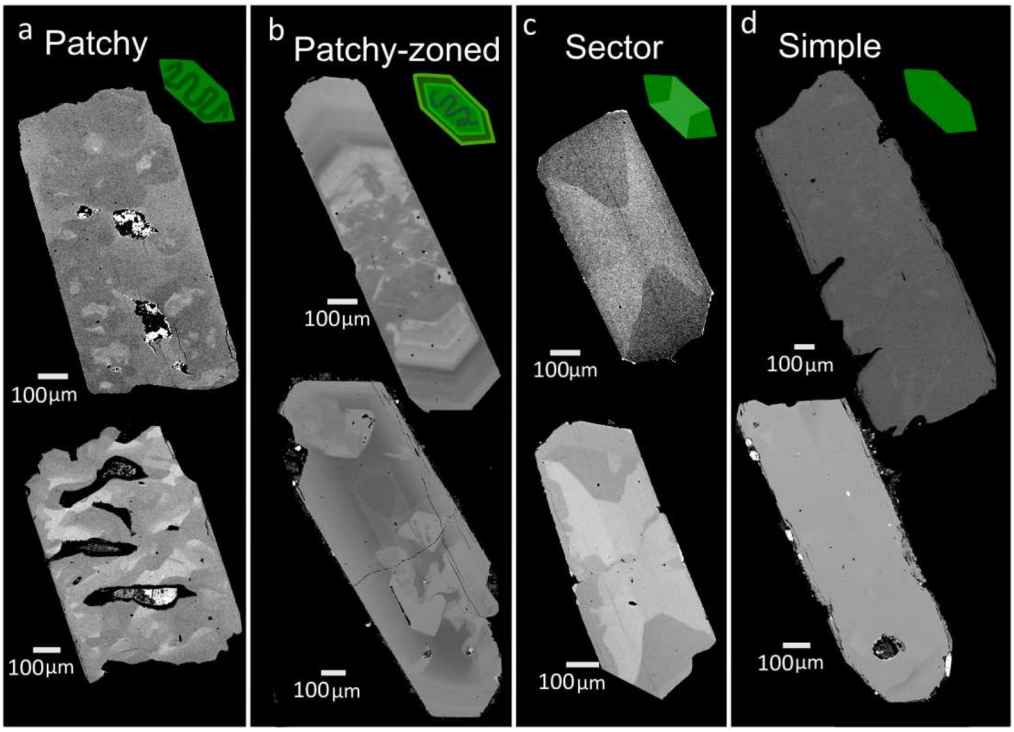

Fig. 3 Images of clinopyroxene phenocrysts in back scatter electron images (BSE). **a** shows the zoned-patchy combination, **b** shows the sector zoning, **c** shows simple or homogeneous crystals, and **d** shows patchy zoning. Each figure has a stylized model of the zoning type, to be used in further figures

VSN0 shows the most chemical variability with ranges of 0.47–0.94 Mg#, 42.76−54.37 wt.% SiO_2, and 1.08−8.81 wt.% Al_2O_3 (Fig. 4). However, the distribution of composition of clinopyroxene in this unit is bimodal. One group has low Mg# (avg = 0.57), SiO_2 (45.75 wt.%), CaO (23.42), MgO (9.28), Cr_2O_3 and NiO below detection limit and high FeO (12.40), Al_2O_3 (6.43), MnO (0.49), TiO_2 (1.24), and Na_2O (0.63). The second group is characterised by high in Mg# (0.90), SiO_2 (avg = 52.64 wt.%), CaO (24.66), MgO (16.39) and low in FeO (3.35) TiO_2 (0.42), Al_2O_3 (2.19), MnO (0.06), Na_2O (0.12), and variable in Cr_2O_3 (up to 0.8) and NiO (0.03), though these elements

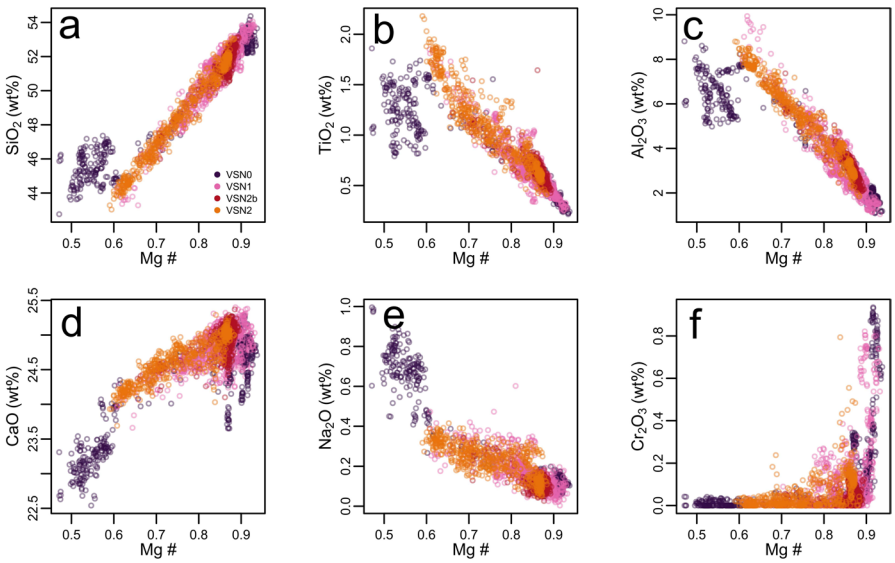

Fig. 4 **A**–**F** Major elements of analyzed clinopyroxene for VSN0 (purple), VSN1 (pink), VSN2b (red), VSN2 (orange) with respect to Mg#. Data can be accessed in Supplementary Data

are low so may be at or close to the limits of the machine sensitivity.

The high SiO_2 clinopyroxene group in VSN0 overlaps with the high end of the VSN ignimbrite units (VSN1 + VSN2b + VSN2; Fig. 4). Within the VSN ignimbrites clinopyroxene from VSN2 generally have lower SiO_2 and Mg# while those from VSN1 have higher values of SiO_2 and Mg#, overlapping with those of clinopyroxenes from the VSN0 group (Fig. 4). Clinopyroxene crystals with Cr_2O_3 >0.25 wt.% and Mg# > 0.8 constitute 26 % and 13% of VSN0 and VSN1 analyses, 0% of VSN2b analyses, and 3% of VSN2 analyses. We define these as high Mg# and high Cr_2O_3 clinopyroxene in further discussion.

Chemical variability by texture

The four textural groups of clinopyroxene we defined above, (1) patchy, (2) patchy-zoned, (3) sector zoned, and (4) simple, show variation in major element space. Of particular note is the low Mg#, CaO, SiO_2 and high FeO, Al_2O_3, Na_2O, and TiO_2 clinopyroxenes from VSN0 (Fig. 5a and i) which are almost all patchy texture (with the exception of a single simple crystal, which is possibly a fragment, Fig. 5l). However, only 10 out of 43 patchy clinopyroxenes have this composition, the rest of the crystals are similar to the other textures in terms of Mg#, SiO_2, and CaO.

High Mg# and high Cr_2O_3 clinopyroxene are primarily simple clinopyroxene (Fig. 5d). There are 23 out of 49 simple textured clinopyroxenes with analyses with Cr_2O_3 >0.25 wt.% and Mg# > 0.8. The rims of the simple textured clinopyroxene show no systematic variation.

Patchy-zoned crystals (Fig 5b,f,j) show minimal systematic variation between the patchy cores and zoned rims. The mean rim relative to the patchy core increases on average by 0.1 wt.% TiO_2, 0.3 wt.% Al_2O_3, and 0.4 wt.% FeO and decreases by 0.5 wt.% SiO_2, 0.3 wt.% MgO, and 0.1 wt.% CaO, and negligible change in all other elements. We note that several crystals show oscillatory zones in a single rim section and thus, the average may not be representative. Chemical profiles of all crystals are available as Supplementary materials.

Sector zoned clinopyroxene have generally high Mg# (avg = 0.85) and Cr_2O_3 content, with 4 out of 7 crystals with analyses in the high Mg# high Cr_2O_3 range (Fig. 5c, g, k). The hourglass sector has lower content in Al_2O_3 (avg = 2.1 wt%), FeO (2.2 wt%), TiO_2 (0.3 wt%), Na_2O (0.1 wt%), and higher SiO_2 (avg = 2.5 wt%), MgO (2.2 wt%), CaO (0.2 wt%) and Cr_2O_3 (0.1 wt%), with respect to the prism sector.

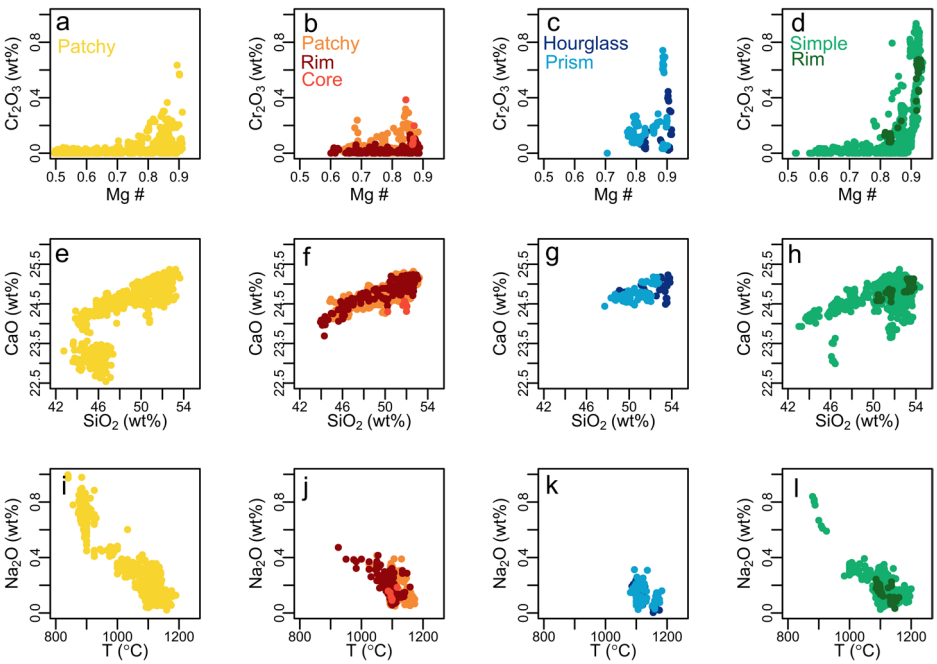

Fig. 5 Mineral compositions separated by textural types. **a–d** shows Mg# versus Cr_2O_3, **e–h** shows SiO_2 versus CaO, and **i–l** shows temperature versus Na_2O. **a**, **e**, and **i** Show patchy textured clinopyroxene in yellow points. **b**, **f**, and **j** show patchy zoned clinopyroxene in orange tones. The light orange is the patchy sections of the crystals, the dark orange is the outer rims, and the vibrant orange shows the unzoned cores, which are only present in a few crystals. **c**, **g**, and **k** show the sector zoned clinopyroxene where the dark blue represents the hourglass sector and the light blue is the prism sector. **d**, **h**, and **l** show simple textured clinopyroxene in light green. The dark green points are the points where there is an outer rim on the crystal

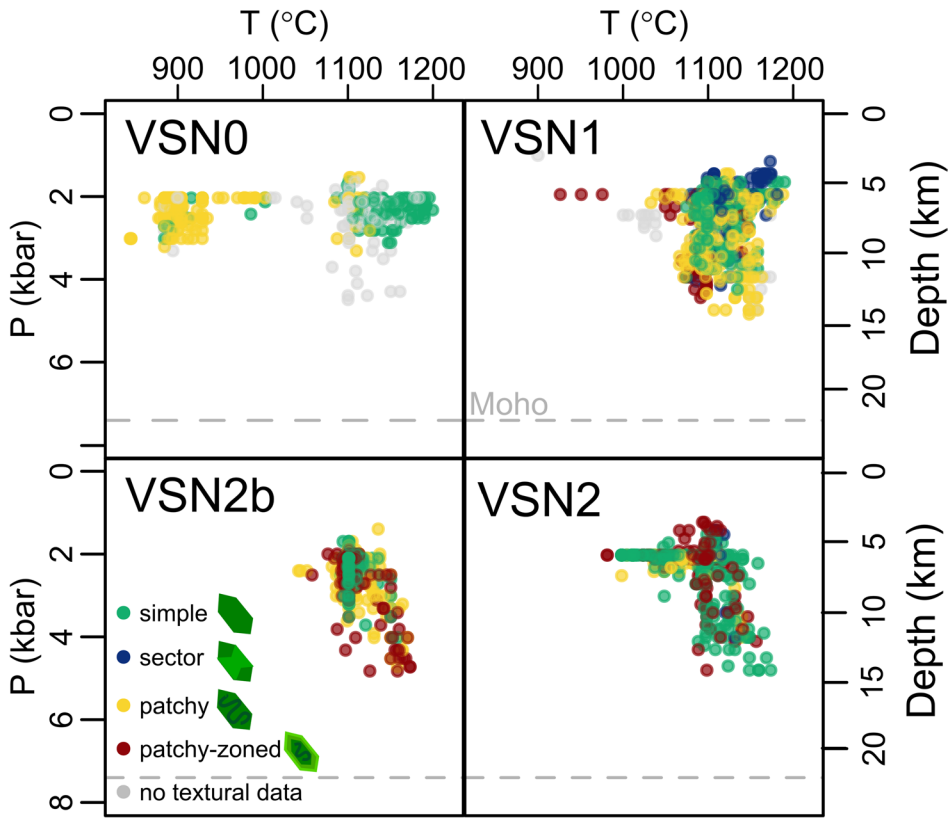

Fig. 6 Pressure and temperature estimates from each subunit. Points are colour coded for the textural type. SEE is 3.2 kbar and 72.5 ° C. See online version for colours

Clinopyroxene Sr and Nd isotopes

A wealth of studies have been carried out on the isotopic compositions and trace element chemistry of CA volcano and the Roman Magmatic Province, but few have specifically focused on the Villa Senni eruptive unit (Boari et al. 2009; Conticelli et al. 2002; Gaeta et al. 2006; Federico et al. 1994). Here we report new Sr and Nd isotopic measurements on clinopyroxene mineral separates of the VSN0 and VSN1 subunits. For these analyses we select crystals with the highest Mg# to minimise any possible impact of crustal contamination. The results show that the clinopyroxene isotopic ratios are within the range of the Roman Magmatic Province ($^{87}Sr/^{86}Sr$ 0.7089–0.7107 and $^{143}Nd/^{144}Nd$ 0.5121–0.5122, Fig. 7a) (Conticelli et al. 2002). Together, Sr and Nd isotope compositions indicate a contribution from an enriched source (high radiogenic Sr and low radiogenic Nd), relative to the depleted mantle (DM) and the mantle array (Salters and Stracke 2004; Conticelli et al. 2015). In the Nd versus Sr isotope space, the clinopyroxene samples define a subhorizontal trend with a range of variability in $^{87}Sr/^{86}Sr$ values (2.5 ‰) that is more than one order of magnitude higher than that in $^{143}Nd/^{144}Nd$ (0.2 ‰). We also note a slight correlation between the clinopyroxene major element chemistry and $^{87}Sr/^{86}Sr$, where at the lowest $^{87}Sr/^{86}Sr$ the Cr_2O_3 is highest and at the highest $^{87}Sr/^{86}Sr$ the Mg# is the lowest (Fig. 7b). Notably, the $^{87}Sr/^{86}Sr$ values of the VSN1 clinopyroxene are systemically higher than the high Mg# clinopyroxene of VSN0.

Clinopyroxene thermobarometry

Results from clinopyroxene thermobarometry indicate clinopyroxene crystallization between 1.2−4.9 kbar (~ 3–15 km, SEE = 3.2 kbar), with most of the distribution centred around 2 kbar (Figs. 6 and 8). Only 18% of the estimates are >3 kbar (8% of VSN0, 32% of VSN1, 14% of VSN2b, and 13% of VSN2). However, we note that due to the large SEE we are unable to resolve details of magmatic reservoirs in the upper crust. Temperature estimates range from 839 to 1200 °C (SEE = 71.9 ° C). However, the largest proportion of estimates is centred around 1100 °C. If we use 1000 ° C as a cut off for high T and low T crystals, we find that 93 % of the estimates are high T. Within subunits VSN0 has 62% high T estimates, and VSN1, 2b and 2 have >99 % high T estimates (Fig. 6).

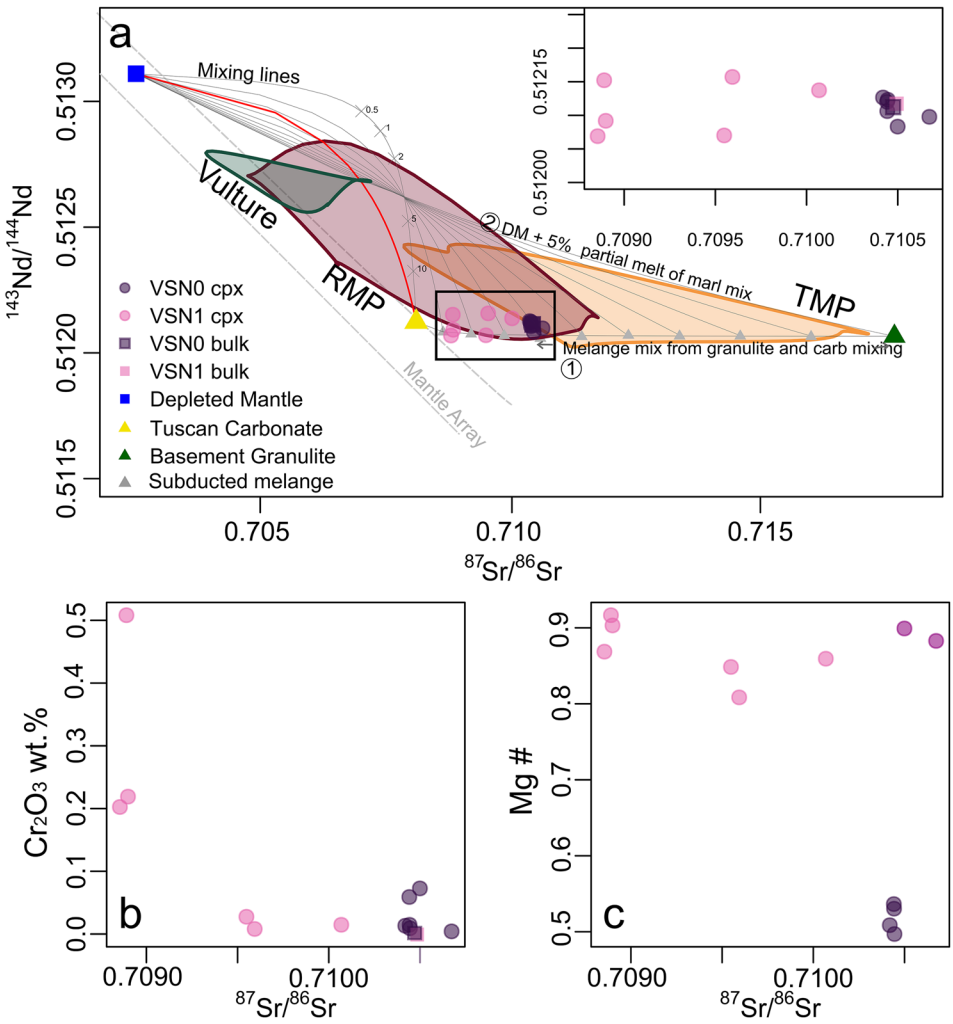

Fig. 7 **a** $^{87}Sr/^{86}Sr$ and $^{143}Nd/^{144}Nd$ signatures for the Colli Albani (pink and purple circles, and in inset plot), the Roman Magmatic Province (RMP), the Tuscan Magmatic Province (TMP), Vulture volcano are outlined as polygons. A depleted mantle (DM) is used as the source material (blue square; Caro and Bourdon 2010; Conticelli et al. 2015). Tuscan limestone used as a proxy for shallow carbonate (yellow triangle; Conticelli et al. 2009) is mixed with DM in the red line. Representative basement for Colli Albani (yellow triangle; Conticelli et al. 2009) mixed with the carbonate and subsequently mixed with DM at regular intervals (grey lines show mixing with 5% partial melting). Grey dashed lines indicate the mantle array as outlined by Carrasquero et al. (2018). $^{87}Sr/^{86}Sr$ variation plotted against **b** Cr_2O_3 and **c** Mg#. Mixing is done using the DePaolo (1981) mixing model

Discussion

Clinopyroxene variability across VSN

VSN0

VSN0 is overwhelmingly the most diverse unit both in terms of geochemistry and P-T estimates. VSN0 shows the full compositional variability of the VSN ignimbrite clinopyroxenes, and shows a bimodal distribution in Mg#, SiO_2, and Na_2O space (Figs. 4, 6). The clinopyroxenes which are low in SiO_2, MgO, CaO, and high in FeO, Na_2O, and MnO are only found in VSN0 and only for patchy textured crystals (Fig. 4). These clinopyroxene give the lowest temperature estimates. As reported in Gaeta et al. (2006) and Palladino et al. (2001) CA magmas do not follow a classical liquid line of descent and evolve with an increasing silica content, as the melts are plagioclase free, and leucite, clinopyroxene, and phologpite bearing. Instead, Na_2O can be used as a differentiation index for these magmas. Thermobarometric estimates for Na_2O-rich patchy clinopyroxenes show that they crystallised at the lowest temperature and mostly at low pressures (Fig. 6). We suggest that these crystals formed from a magma emplaced into a shallow cold crust that interacted with shallow carbonates. Likely these clinopyroxenes are picked up on the margins of the magmatic reservoir during the eruption. Patchy clinopyroxenes in the literature are associated with diffusion limited crystal growth and subsequent overgrowth via magma mixing or reheating and are associated with depleted Na_2O. Our patchy clinopyroxenes are bimodal in Na_2O space, similar to the works of Brehm and Lange (2020); Welsch et al. (2016). We also note a lack of rims for the patchy clinopyroxene, which indicates that these clinopyroxenes were likely not exposed to the last recent recharge event before eruption. VSN0 clinopyroxenes also show the widest range in temperature (Fig. 6). Texturally, high T VSN0 clinopyroxenes are all simple. The high T clinopyroxenes are also those with the highest Mg# and Cr_2O_3 content. We suggest these crystals have crystallized

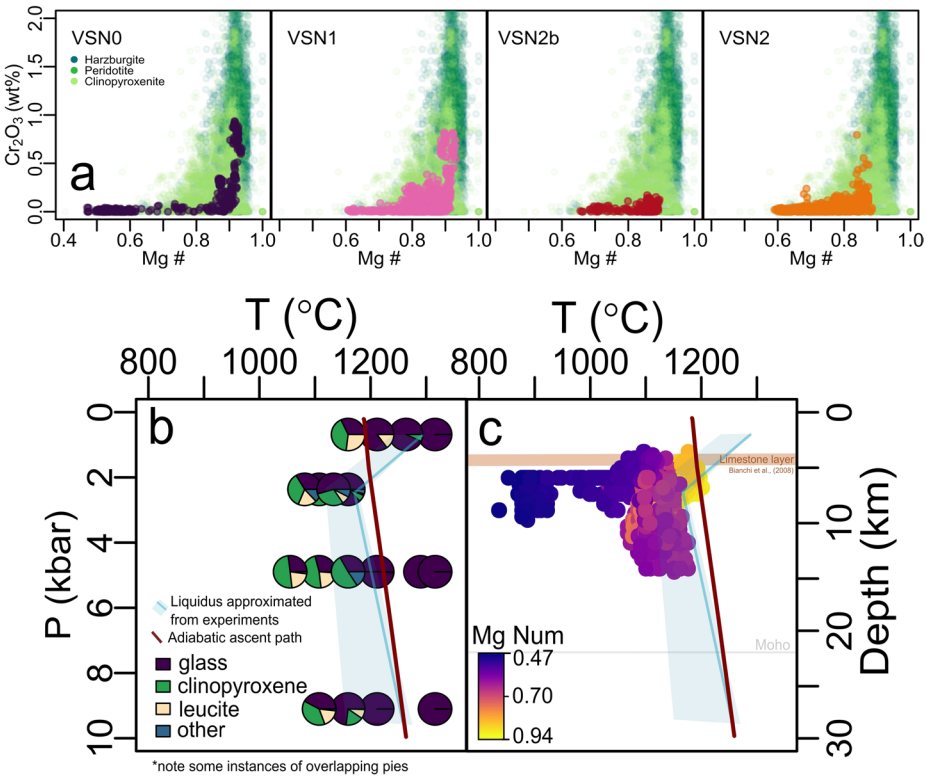

Fig. 8 **a** Magnesium number (Mg/(Fe + Mg)) with respect to Cr_2O_3 for the crystals of VSN as well as typical mantle clinopyroxenes from GEOROC (green points). **b** Approximated liquidus (blue line) from phase equilibria experiments. The pie charts provide the phase and their relative proportions for each experiment. The red line represents an adiabatic ascent path from MELTS, as described in the Methodology (Gualda and Ghiorso 2015; Ghiorso and Sack 1995; Asimow and Ghiorso 1998). **c** Pressure and temperatures estimates as generated by the random forest thermobarometer, colour coded for magnesium number (Jorgenson et al. 2022) and overlaid by the adiabatic ascent path and liquidus as in **b**. SEE is 3.2 kbar and 71.9 ° C

shortly before the eruption directly from a mantle derived melt.

VSN1

VSN1 has a fairly broad distribution in P-T space with pressures from 1.2 to 4.9 kbar and temperatures from 925 to 1192 °C, however, we note that these P estimates are almost within error (Fig. 6). Geochemically, VSN1 spans a wide range in SiO_2, Mg#, and CaO, and shows all texture types (patchy, patchy-zoned, simple, and sector zoned, as seen in Fig. 6). The variability in clinopyroxene geochemistry of these crystals as well as the wide range in temperature estimates and textural variability are indicative of a mixture of crystals showing a protracted residence in the shallow portions of the plumbing system and crystals formed shortly before eruption.

The cores of the patchy-zoned clinopyroxene have the same composition of the patchy textured clinopyroxenes (Fig. 5). We also note that VSN1 does not have any of the patchy low temperature, low SiO_2, high FeO and high Na_2O clinopyroxenes observed in VSN0.

Notably, VSN1 has almost all of the sector zoned clinopyroxene. Sector zoning is a texture that is oft associated with rapid crystal growth (Ubide et al. 2019; Brehm and Lange 2020). Welsch et al. (2016) demonstrates that enrichment or depletion of elements in the hourglass and prism zoned sections is cause of growth rate and supersaturation, as seen in their suite of clinopyroxenes from Haleakala volcano (Hawaii). They attribute an enrichment in Al, Ti, and Na and depletion in Si, Mg, Ca, and Cr in the {-111} to rapid growth at depth with a high supersaturation in the reservoir. They suggest the inverse (Mg, Ca, Si rich and Al, Ti, Na, and Cr poor in the {-111} sector) is indicative of slow growth at the surface implying low supersaturation in a lava flow. Within the literature there is some variation in sector zoning trends where Ubide et al. (2019) notes an enrichment in Si and Mg and depletion in Al, Fe, and Ti in the {111} sector for Etna and alkaline trachybasalts clinopyroxenes, and Welsch et al. (2016) notes the opposite for alkalic basalt from Haleakala. Neave et al. (2019) focused on tholeiitic magmas from Holuhraun lavas, Iceland and found results in closer agreement to Ubide et al. (2019) where the {111} sector is enriched in EnFs (Fe and Mg rich) clinopyroxene component at the expense of DiHd and CaTs (Ca and Al rich) components. The discrepancy may be related to magma compositions. Regardless, our results closely resemble those of Ubide et al. (2019).

VSN2 and VSN2b

VSN2b and VSN2 show less variability in the temperature range, with no estimates below 1000 °C (Fig. 6). Geochemically, these clinopyroxenes tend to have a higher SiO_2 on average. Texturally, both subunits show simple, patchy, and

patchy-zoned textures. As with VSN1 the presence of these textures is indicative of several instances of magma mixing, and different phases of equilibrium and disequilibrium in the crystal's history. The smaller proportion of high Mg#-Cr_2O_3, high temperature, simple textured clinopyroxenes (Figs. 4f and 6) is indicative of a waning input of the mafic magma present at the onset of the eruption (VN0 and VSN1) This is also seen between VSN2b and VSN2 where average and max Mg# decreased from 0.86 and 0.89 in VSN2b to 0.88 and 0.76 in VSN2.

Assimilation induced $^{87}Sr/^{86}Sr$ and $^{143}Nd/^{144}Nd$ isotopic variability

There has been significant work done to assess the role of carbonate assimilation via isotopic analysis for the Roman Magmatic Province, with most evidence converging to a metasomatized mantle source (Gaeta et al. 2006; Conticelli et al. 2015; Avanzinelli et al. 2009). There is, however, a lack of isotopic work on the VSN eruption at CA, and specifically the isotopic compositions of mineral phases, save a few crystals measured in a regional study of Gaeta et al. (2006). In order to evaluate the role of carbonate assimilation for the VSN eruption, we present $^{87}Sr/^{86}Sr$ and $^{143}Nd/^{144}Nd$ isotopic signatures specifically from clinopyroxenes with high Mg# and Cr_2O_3, as these clinopyroxenes should have crystallized from the most primitive magma and thus should provide the closest approximation of the magmatic source. These signatures define a sub-horizontal trend in the Nd versus Sr isotope space, where VSN0 clinopyroxenes have higher $^{87}Sr/^{86}Sr$ values than the VSN1 clinopyroxene. The sub horizontal trend is likely caused by mixing between two sources, characterized by different $^{87}Sr/^{86}Sr$ ratios, one >0.7107 and the other <0.7089, and by a similar $^{143}Nd/^{144}Nd$ (~0.5121−0.5122). Our data lay well within the region of the Roman Magmatic Province (Fig. 7a) and agree with whole rock $^{87}Sr/^{86}Sr$ (0.710570−0.710673) and $^{143}Nd/^{144}Nd$ (0.512095−0.512117) shown in Boari et al. (2009).

While there are several works which have looked in greater detail at the magmatic source of the Roman Magmatic province, including Gaeta et al. (2006); Conticelli et al. (2002, 2015); Avanzinelli et al. (2009, 2018) and Conticelli et al. (2010), here we find merit in a step by step process of elimination to evaluate the source. We start with a depleted mantle source and consider several options of assimilation and metasomatism to produce the enrichment of primitive magma that is observed in all the Roman Magmatic Province. We broadly consider four possible scenarios for enrichment of a depleted mantle through a long timescale of mixing, where the first three address assimilation of various crustal lithologies at variable crustal levels by a depleted mantle-derived primitive magma. Here we use a depleted mantle source to test the possibility that the enrichment of the primitive magmas of the Roman Magmatic Province occurs at crustal level and not in the mantle. The fourth situation looks at enrichment processes occurring in the mantle source of the magmas. Parameters used for this model can be found in the supplementary materials.

Models involving deep to shallow crustal assimilation by mantle-derived magmas

One possibility to explain the clinopyroxene signatures could be assimilation of regional Meso-Cenozoic carbonate rocks by a primitive magma derived from partial melting of a depleted mantle (Fig. 7, red line). However, none of the highly radiogenic $^{87}Sr/^{86}Sr$ values of the clinopyroxenes of the CA volcano can be obtained by simple carbonate assimilation because the Sr isotope signature of Meso-Cenozoic carbonates are less radiogenic than the $^{87}Sr/^{86}Sr$ values of all analysed clinopyroxenes analysed (Boari et al. 2009). Additionally, even approaching the isotope signatures of the clinopyroxenes through such a process would require unreasonable amounts of carbonate assimilation (>80 %) at shallow crustal levels. This is the consequence of the high Sr concentrations of both mantle-derived magma rocks (1019–2747 ppm) and clinopyroxenes (up to 3640 ppm), which make them insensitive to crustal contamination as crustal rocks are characterized by much lower Sr contents (avg Sr = 314 ppm) (Conticelli et al. 2015; Gaeta et al. 2016; Boari et al. 2009; Shaw 2018).

Another possibility could be mixing of a depleted mantle-derived basalt with bulk material or partial melts of regional metamorphic and sedimentary rocks of CA (gneiss, granulite, flysch, pelite, travertine, schist, marl, and limestone; Hirschmann et al. 2008). As the clinopyroxenes have a high Sr concentration, and should crystallize from a magma with a high Sr content, we model low degrees of partial melting of the regional rocks (0–5%) to maintain a high Sr concentration in the crustal material mixed with mantle-derived basalt. However, we found that none of these mixing compositions could satisfactorily fit the full spread of the VSN clinopyroxene isotopic signatures (Fig. 11a).

A third possibility could be a two-step mixing process in which a DM-derived primary magma assimilates granulitic rocks in the lower crust and subsequently mixes with carbonate rocks in the shallow crust (Fig. 11b). In this model the DM-derived primitive magma is initially mixed with 5% partial melt of granulite up to a ratio of DM-derived magma/granulite partial melt of 5:1 to obtain the low radiogenic $^{143}Nd/^{144}Nd$ compositions of the clinopyroxenes (0.5121−0.5122). Then, the hybrid magma (DM-derived primary basalt and 5% partial melt of granulite in a ratio 5:1) assimilates carbonates in the shallow crust. This model allows us to reproduce the subhorizontal trend in the Sr-Nd isotope

space, but requires again unrealistic assimilation of >80% carbonate rocks at shallow level to reproduce the VSN clinopyroxene $^{87}Sr/^{86}Sr$ values (Fig. 11b).

Furthermore, if upper crustal carbonate assimilation was responsible for the isotopic variability measured in clinopyroxene, we should observe a decrease in $^{87}Sr/^{86}Sr$ with decreasing Mg# and Cr_2O_3, which is not observed in our data (Fig. 7b, c). On the basis of the above discussion, we discard assimilation of carbonates and other crustal rocks at variable crustal levels as a cause of the isotopic variability measured in the clinopyroxenes (Conticelli et al. 2015; Gaeta et al. 2016; Boari et al. 2009; Barbieri et al. 1979).

Model involving mixing of partial melts of isotopically distinct mantle domains

The most likely explanation for the linear trend defined by the CA clinopyroxenes in the Sr-Nd isotope space is mixing in variable proportions of partial melts of two different metasomatized mantle portions. Figure 7a shows that end members with suitable compositions for such mixing can be obtained through previous metasomatism of a depleted mantle by small proportions of partial melts of subducted melange or marl, which has been thoroughly investigated by Avanzinelli et al. (2008) and others (Conticelli et al. 2009, 2015; Conticelli 1998; Conticelli et al. 2007; Federico et al. 1994; Gaeta et al. 2006). We also note the works of Gaeta et al. (2006), who reports $^{87}Sr/^{86}Sr$ from clinopyroxene throughout the entire eruptive history, including 6 clinopyroxene from VSN unit with variable Mg# ($^{87}Sr/^{86}Sr$ 0.710452−0.710525, within range of our samples). They find a strong temporal variation, where $^{87}Sr/^{86}Sr$ decreases with time. The sub-horizontal trend between the VSN0 and VSN1 $^{87}Sr/^{86}Sr$ values, is in line with their hypothesis that the temporal variability is caused by a progressive depletion of the metasomatized veins of the mantle source region. Several studies also suggest that the partial melt of this heterogeneous mantle source is strongly silica undersaturated, potassic, and rich in CO_2 (Conticelli et al. 2015; Avanzinelli et al. 2008).

Explosivity linked to shallow carbonate assimilation?

Many studies regarding CA centre on the role of additional CO_2 from shallow carbonate assimilation to cause the anomalous behaviour and present day geophysical evidence points to a magma reservoir within Meso-Cenozoic carbonate sediments (Freda et al. 2008, 2011; Iacono-Marziano et al. 2007; Mollo et al. 2010; Bianchi et al. 2008). Several studies focus on the Pozzolane Rosse (RED) ignimbrite as it has abundant carbonate clasts in the deposit, whereas fewer are present in the upper ignimbrite units PNR and VSN. Additionally, the carbonate clasts in RED have reaction rims showing de-carbonation, resulting in the growth of fragile dendritic pyroxenes in cavities sometimes occupying the core of a completely consumed carbonate clast (Fig. 1b). It is unlikely that the carbonate reaction occurred at depth and such fragile structures resisted deposition in high energy pyroclastic flows. Furthermore, in very distal deposits at >30 km from the volcanic centre, carbonate clasts are not reacted (Calabró et al. 2022). Emplacement temperatures at the proximal and medial localities are estimated to be >630 ° C and distally >580 ° C (RED09 and RED01 respectively in Trolese et al. 2017). The onset of carbonate reaction is at temperatures ranging from 600 to 650 ° C, which may explain why the hotter proximal carbonate clasts are reacted whereas the distal and cooler carbonate clasts show a smaller reaction progression (Floess et al. 2015; Wyllie and Tuttle 1960). Additionally, proximal to the volcanic centre within RED, there are many large degassing pipes (Fig. 1c) which become smaller and less abundant distally. We suggest these pipes originate from excess CO_2 liberated in-situ during decarbonation of the carbonate clasts. This evidence suggests that the reaction of carbonates occurred mostly after the emplacement of the pyroclastic density currents and it is not per se evidence of carbonate assimilation over the time span of magma accumulation in the shallow reservoir.

Even if we argue that the presence of carbonate clasts are not proof of carbonate assimilation during magma accumulation, assimilation of carbonates could still occur. However, we argue that this process would not trigger a sustained caldera forming eruption. Experiments by Freda et al. (2011) show that a 1 mm^3 carbonate clast in a phono-tephritic melt at 1200 °C, 0.5 GPa, and 2.5 wt.% H_2O, resorbs almost completely after 60 s. The magma assembly timescales we calculate are orders of magnitudes longer than the decarbonation timescales. Thus, because the CO_2 solubility at upper crustal depths is low (Vetere et al. 2014) and because of the extremely low viscosity of magma at CA, the excess CO_2 generated during decarbonation would rapidly leave the reservoir. Even if the increase of volume associated with decarbonation could serve to increase the overpressure within the reservoir to critical value, the rapid decoupling of excess volatile phase and magma would not permit a sustained eruption as observed at CA (Moussallam et al. 2015). Several authors (Knuever et al. 2022; Freda et al. 2011) have suggested syn-eruptive decarbonation could provide an additional mechanism to increase explosivity. However, because of the sustained nature of the eruption, the rate of assimilation should stay relatively constant throughout the eruption,

which is difficult to imagine for the entire course of all seven of the large volume eruptions in CA's history. However, such short lived CO_2 contributions however may be the driving force behind the short lived and small volume eruptions such as the Peperino Albano eruption (Cross et al. 2014).

Magma accumulation

Variation in P-T space

As seen in Fig. 8 the P–T estimates span a large range from 839 to 1200 ° C and 1.2–4.9 kbar. VSN0 patchy clinopyroxenes are generally low temperature and we propose these are the oldest crystals, having emplaced into a cooler crust, differentiated, and faced several instances of disequilibrium, giving them the patchy texture. The bulk of the clinopyroxene from VSN1, VSN2b, and VSN2 record much higher temperature (around 1100 °C). The highest temperature estimates are from VSN0 and VSN1, and up to 1200 °C. We suggest that the increase of clinopyroxene recording high temperature observed through the eruptive sequence is evidence of the progressive increase of the contribution of high temperature magma to the erupted products (Fig. 6).

Evidence for Rapid accumulation

Considering that 99% of clinopyroxene crystals of the ignimbrite record temperature in excess of 1000 °C, we can estimate the duration of magma storage at shallow depth if we define plausible temperature of magma injection and for the upper crustal rocks. For the temperature of magma input we consider the highest temperature recorded by clinopyroxene (i.e. 1200 °C). Additionally, to obtain the maximum possible duration of magma storage in the shallow crust, we consider that magma input occurred in a reservoir with magma at a temperature of 800 °C, the minimum temperature we estimate from thermometry (Fig. 6). We use a simple 1D thermal model and consider a lens of magma of 360–60 m thickness using a radius for the footprint of the magma reservoir of 4 and 10 km and an erupted magma volume of 18 km^3 DRE, at 1200 °C (the maximum temperature estimates) embedded in a magma at 800 °C (the minimum estimated temperature; Fig. 8; Giordano 2010). The results show that to maintain magma in excess of 1000 °C (which we consider eruptible) at shallow crustal depth, the reservoir could not have been active for more than 70–2260 years (for thicknesses of 360 and 60 m, respectively). This is a maximum estimate as it represents the time at which the maximum temperature within the lens, originally at 1200 °C, drops below 1000 °C and also because the ambient temperature is 800 °C, which is extremely high for the upper crust and only attainable if an upper crustal reservoir was established at depths of few kilometers. We note this assumes that the entire reservoir is evacuated, which is a reasonable estimate considering the works of Geyer et al. (2006), which indicate that for a low aspect ratio magma reservoir approximately 20 volume % is needed to initiate caldera collapse. This amount would represent the VSN1 volume and since VSN2 is more voluminous than VSN1 the net volume fraction erupted is likely close to all of the magma. Our results and calculations suggest that the upper crustal reservoir was assembled at accumulation rates in excess of 0.1 km^3/years and was finally destabilized by the rapid input of magma directly from the mantle.

Rapid magma ascent from the mantle and an alternative trigger mechanism

High Mg# clinopyroxene from shallow depth

The subgroup of clinopyroxene with high Mg# and high Cr_2O_3 are most commonly found in the simple textured clinopyroxenes (Fig. 8) and return temperature estimates of up to 1200 °C. High Cr_2O_3-Mg# clinopyroxene also record pressures of about 2 kbar (~6 km, Fig. 8). This at first is a non-intuitive result in that such a high Mg# and Cr_2O_3 indicates these are the most primitive clinopyroxenes of the Villa Senni eruption and thus should crystallize from the deepest melt, however, our results give low crystallization pressure estimates. We suggest that this is due to rapid ascent of mantle derived magma, which only starts crystallising once significant amounts of H_2O is released from magma at relatively shallow depth (Fig. 8b, c). In fact, the quasi-adiabatic ascent of a magma produced in the mantle will results in the magma being overheated until significant water is released from the system and the magma starts to crystallise (Fig. 8; Hamilton et al. 1964; Metrich et al. 2001; Plank et al. 2013; Papale et al. 1999).

We used phase equilibrium experiments from the literature to approximate the liquidus by plotting phase proportions on a pressure-temperature diagram, as seen in Fig. 8b. Most phase equilibria experiments of CA are focused on the Mt. Mellone lava flows, which is a plagioclase free phonotephrite (Freda et al. 2008; Iacono-Marziano et al. 2007). There is one study from Freda et al. (1997) which used a starting composition of VSN, though it does not give relative phase proportions. Mollo et al. (2010) use a synthetic primitive glass based on the Roman Magmatic Province. Data at <2 kbar are anhydrous whereas all other experiments have at least 1 wt.% H_2O and a range of CO_2 (added as $CaCO_3$ or

$CaMgCO_3$) and f_{O2}. These difference results in a range of liquidus temperatures (shaded region in Fig. 8).

We consider the liquidus temperature of magmas from CA at the base of the crust (approximately 25 km; Giordano and Caricchi 2022) and trace an adiabatic ascent path from this depth (as calculated from MELTS with a bulk composition of SiO_2 45.88, TiO_2 0.75, Al_2O_3 18.67, Fe_2O_3 0.0, Cr_2O_3 0.0, FeO 6.53, MnO 0.20, MgO 1.37, NiO 0.0, CoO 0.0, CaO 7.77, Na_2O 4.46, K_2O 6.27, and P_2O_5 0.22, normalized to include 2 wt.% H_2O and 1 wt.% CO_2 and started from 1250 ° C and 10 kbar; Gualda and Ghiorso 2015; Ghiorso and Sack 1995; Asimow and Ghiorso 1998). The adiabatic ascent path intercepts the fluid saturated liquidus in correspondence with the high temperature cluster of temperatures estimated from clinopyroxene (Fig. 8). This supports our hypothesis that high Mg# and Cr_2O_3 clinopyroxenes (11.5% of analyses) are the results of input of primitive magma from depth.

Rapid ascent trigger

Clinopyroxene chemistry and thermobarometric estimates us to draw a series of conclusions on process preceding the Villa Senni caldera forming eruption. The clinopyroxenes of VSN0 fall deposit are distinctively different from those of all other subunits of the ignimbrite. Estimated temperature of VSN0 below 1000 °C make up 38% of analyses (n = 163), while this value is lower than 1% for all other subunits. Additionally, temperature estimates in excess of 1150 ° make up 16% and 13% of the VSN0 and VSN1 analyses but only 6% and 2% for VSN2b and VSN2. Additionally, temperature estimates above 1000 °C make up >99% of the VSN ignimbrite estimates. We suggest that VSN0 was produced by the rapid ascent (quasi-adiabatic) of magma from depth that collected clinopyroxene antecrystals (returning low temperature estimates) through the entire plumbing system with minor or no crystallisation upon ascent because of the overheated nature of the magma. The eruption of the VSN0 subunit causes the destabilization of the entire upper magma reservoir and the initiation of the caldera forming eruption. This is in contrast with the proposition that CO_2 from carbonate assimilation in the upper crust is the driving mechanism of the eruption (Freda et al. 2011; Iacono-Marziano et al. 2008). Experimental work from Freda et al. (2008), which simulates carbonate assimilation of CA magmas results in low Mg# (0.48–0.62) and low Cr_2O_3 (0.0–0.23 wt.%) clinopyroxene. However, our results show that the eruptive products contain high Cr_2O_3-Mg# clinopyroxenes, with the great majority of clinopyroxene having Mg# above 0.62 (Fig. 8a). Additionally, the great majority of clinopyroxene return temperature estimates in excess of 1000 ° C implying short storage at shallow depth as discussed in Sect. 4.4.2.

Magma injection is a well established trigger mechanism in the literature, including examples from Pinatubo 1991 eruption and the 3.6 ka Santorini eruption (Caricchi et al. 2021; Pallister et al. 1992; Druitt et al. 2012). Magma injection does not always trigger an eruption, as evidenced by caldera systems, and depends on parameters of the recharge itself (rate, magnitude, and style) as well as the state of the current magmatic reservoir (reservoir pressure, magma compressibility, and viscoelastic relaxation rate of the crust; Caricchi et al. 2021; Jellinek and DePaolo 2003; Degruyter et al. 2016). Here, the presence of the VSN0 fall deposit, the lack of clinopyroxene textures indicative of magma mingling (patchy-zoned clinopyroxene) in VSN0, and the presence of the most primitive clinopyroxene in the earliest erupted units, all indicates a lack of significant interaction between magma injected from depth and magma stored in the shallow crust. Thus, magma injection must have quickly cut through the shallow reservoir and destabilized it (similar to Cape Riva at Santorini as in Fabbro et al. 2013), from which the decompression the resident eruptible magma occurred. This agrees with the hypothesis of Vinkler et al. (2012), who proposes VSN0 causes a decompression wave which intersects with a rising foamy magma resulting in a progressively deeper fragmentation level.

The proportional increase in high temperature crystals between VSN0 and VSN1 indicates the increase of the contribution of deep-sourced magma to the eruptive products. This leads to the evacuation of the upper crustal reservoir and the caldera collapse, a rapid process as suggested by the lack of re-equilibration of the high Cr_2O_3 and Mg# clinopyroxene crystals of VSN0. The chemical composition of the magma combined with high temperatures, implies that the magma was of low viscosity, which favour decoupling with the excess volatile phases. Volatile and magma ascent rates have an important role to play in the explosivity of volcanoes (Cassidy et al. 2018; Gonnermann and Manga 2007). For example, the basaltic Cerro Negro erupted magma of the same composition in both 1992 and 1995 but one was effusive and the other explosive, the only difference was that for the effusive event, the outgassing of CO_2 during ascent was more efficient (Roggensack et al. 1997).

Thus, it is clear that to have an explosive event at Colli Albani the magma ascent must be fast enough to be coupled with the volatile phase, or else the eruptive potential of the magma would be lost with the degassing volatiles. This is again in agreement with the works of Vinkler et al. (2012) provide textural evidences indicating rapid ascent. Furthermore, that suggests bubble nucleation is deep, which propels the magma upward rapidly. While determining actual ascent

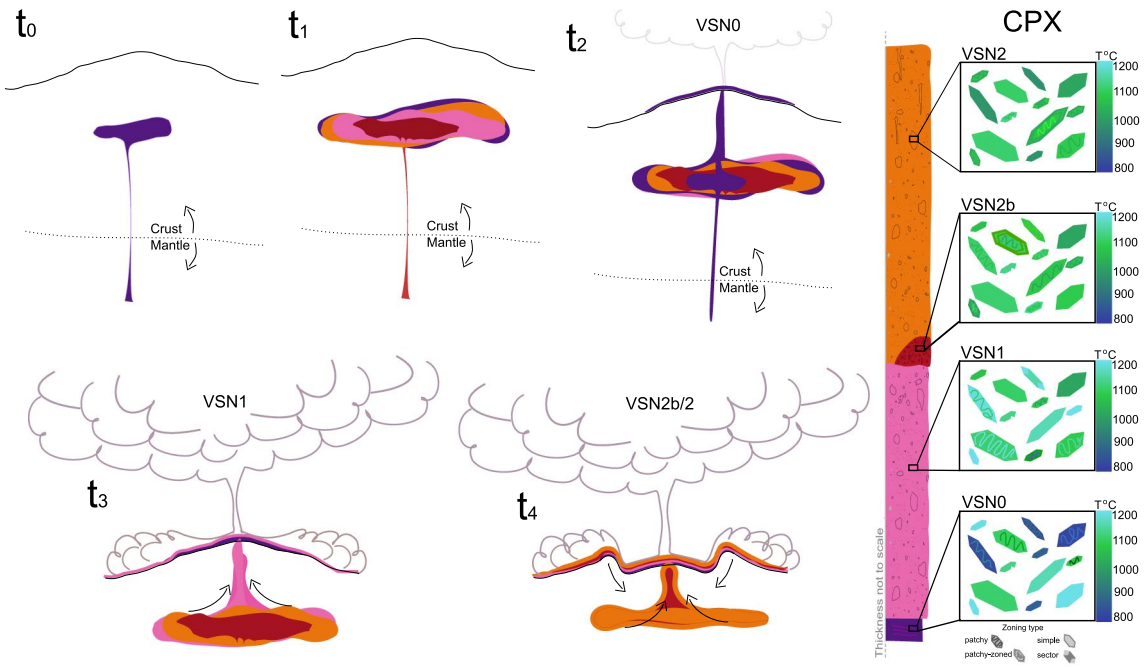

Fig. 9 Schematic (not to scale) diagram to explain the magmatic reservoir assembly and eruption of the VSN eruption. See text for further details

rate is out of the scope of this work, we note the works of Campagnola (2015) who have modelled ascent rates of PNR, another ignimbrite of CA, and estimate the Plinian fallout exit velocities to be as high as 600 m/s and the ignimbrites exit velocities to be 120 m/s.

Eruption sequence

Using our results we reconstruct the sequence of events leading to the caldera forming event that produced the Villa Senni Ignimbrite.

*Pre-eruptive reservoir assembly (t0 in Fig.*9): As CA is a system which has undergone several large volume ignimbrite forming eruptions, which notably occur cyclically, we suggest that at the onset of accumulation of magma for the VSN caldera, there may have been remnants of a previous magmatic reservoir in the upper crustal system from the eruption of PNR. However, our lower temperature estimates from clinopyroxene crystallization give only 800 °C so we suggest the crust was relatively cool when the VSN magma started to accumulate (Fig. 9).

Thermal maturation of assembly (t1): We find evidence of a broad range of temperature estimates from our clinopyroxene thermobarometry. This suggests to us that the magma accumulated in the upper crust via progressive pulses of magma. The assembly of eruptible magma is a rapid process as discussed in 4.4.2, on the order of tens to thousands of years.

Eruption of VSN0 (t2): We propose that instead of stalling in the upper crust, a pulse of magma eventually blew through the crustal reservoir, entraining some low *T* clinopyroxenes which crystallized from the margins of the magmatic reservoir, and erupted to produced the VSN0 unit (Fig. 9, t2). This mixture of cooled and crystal rich magma (low T, patchy clinopyroxene) and the primitive high temperature magma (high T - high Cr_2O_3 and Mg# simple zoned clinopyroxene) explains the two distinct clusters of clinopyroxene chemistry (as discussed in section 4.1.1 and seen in Fig. 9 at the bottom left).

VSN1 and VSN2 eruption (t3 and t4): We suggest that this initial pulse from deep destabilized the rest of the system and allowed for the rest of the VSN eruption to take place. This includes the caldera collapse (Fig. 9 t4) as outlined further in Vinkler et al. (2012) and Giordano (2010). We see variability in sampling represented in the $^{87}Sr/^{86}Sr$ variability between VSN0 and VSN1, where VSN0 is systemically higher in $^{87}Sr/^{86}Sr$ space indicative of sampling different portions of the reservoir. The VSN1 clinopyroxenes are representative of the entire range of temperatures and thus sampled the full range of the clinopyroxene variability in the long standing reservoir as well as the most primitive magmatic pulse. The VSN2b and VSN2 clinopyroxenes give a more uniform temperature distribution, possibly indicative of the eruption of dominantly deep sourced magma during the final phase of the eruption.

Conclusions

Our mineral chemistry and isotopic data together with thermal modelling demonstrate that an upper crustal reservoir was assembled in tens to thousands of years by the repeated injection of CO_2-rich magma produced by partial melting of a metasomatized mantle (Avanzinelli et al. 2008; Conticelli et al. 2009, 2015; Conticelli 1998; Conticelli et al. 2007; Federico et al. 1994; Gaeta et al. 2006). One such recharge event cuts through the upper crustal reservoir erupting crystal-poor primitive magma and carrying a large portion of clinopyroxene antecrysts (VSN0). Such event was rapidly followed by the evacuation of most of the 18 km^3 DRE that constitutes the Villa Senni ignimbrite, and leading to the caldera collapse. We propose that the rapid ascent and accumulation of CO_2-rich and low viscosity magmas from the mantle are responsible for the highly explosive nature of eruptions at CA. This confirms the essential role of magma ascent rate on intensity of eruptions (Ferguson et al. 2016), as is also seen in systems similar to VSN such as the PNR which are thought to have ascent rates in the 100 s of m/s (Campagnola et al. 2016), the Curacautin mafic ignimbrite (Llaima, Chile) was also the result of rapid magma ascent and was released in only 15–17 h (Marshall et al. 2022), and the Cerro Negro (Nicaragua) effusive to explosive transition which is ascribed to volatile loss due to slow ascent speed (Roggensack et al. 1997). In this respect, contrary to the commonly suggested association between explosive eruptions and high viscosity magma, low viscosity and gas-rich magma should be considered prime candidates for eruptions of high intensity preceded by relatively short unrest phases. Because low viscosity favours the decoupling of magma and excess volatiles, high rates of magma ascent are essential for mafic and alkaline magma to erupts explosively.

Our data show that the rapidity of extraction of magma from the mantle is what ultimately drives the sustained eruption of such low viscosity magma as opposed to CO_2 addition from shallow carbonate assimilation. We can envisage the plumbing system as an open system for both melt and gas, where each pulse recharges the shallow reservoir and also provides CO_2 flushing from the mantle region upward as magma migrates. Gas sparging is, therefore, a much more viable mechanism as proposed by Vinkler et al. (2012), that may control both the CO_2 and H_2O contents in the shallow reservoir leading to eruption (Caricchi et al. 2018, 2014). These findings are important for the assessment of volcanic hazard in such highly vulnerable regions. A large caldera forming eruption at Colli Albani would be preceded by the accumulation of magma in the shallow crust in tens to no longer than thousands of years, which would be detectable with geophysical methods. Importantly, such short timescales imply that magma was present in the deepest portion of the magmatic system also during the pauses in volcanic activity, and thus long dormancy does not imply extinction (Giordano and Caricchi 2022).

Supplementary Information The online version contains supplementary material available at https://doi.org/10.1007/s00410-023-02091-z.

Acknowledgements CJ and LC received funding from the Swiss National Science Foundation (grant no. 200021_184632). LC received funding from the European Research Council (ERC) under the European Union's Horizon 2020 research and innovation program (Grant agreement 677493-FEVER). We would like to thank Dr. Sarah Brehm and two anonymous reviewers and the editor Gordon Moore for their feedback.

Funding Open access funding provided by University of Geneva.

Data availability Data is avaliable in the supplementary material.

Declarations

Conflict of interest The authors have no competing interests to declare that are relevant to the content of this article.

References

Aiuppa A, Casetta F, Coltorti M et al (2021) Carbon concentration increases with depth of melting in earth's upper mantle. Nat Geosci 14(9):697–703

Asimow PD, Ghiorso MS (1998) Algorithmic modifications extending melts to calculate subsolidus phase relations. Am Mineral 83:1127–1132. https://doi.org/10.2138/am-1998-9-1022

Avanzinelli R, Elliott T, Tommasini S et al (2008) Constraints on the genesis of potassium-rich Italian volcanic rocks from U/Th disequilibrium. J Petrol 49:195–223. https://doi.org/10.1093/petrology/egm076

Avanzinelli R, Lustrino M, Mattei M et al (2009) Lithos potassic and ultrapotassic magmatism in the Circum-Tyrrhenian region: significance of carbonated pelitic vs. pelitic sediment recycling at destructive plate margins. LITHOS 113:213–227. https://doi.org/10.1016/j.lithos.2009.03.029

Avanzinelli R, Casalini M, Elliott T et al (2018) Carbon fluxes from subducted carbonates revealed by uranium excess at mount Vesuvius. Italy. Geology 46(3):259–262. https://doi.org/10.1130/G39766.1

Barbieri M, Masi U, Tolomeo L (1979) Origin and distribution of strontium in the travertines of latium (central Italy). Chem Geol 24:181–188. https://doi.org/10.1016/0009-2541(79)90121-9

Battistini GD, Montanini A, Vernia L et al (2001) Petrology of melilite-bearing rocks from the Montefiascone volcanic complex (roman

magmatic province): new insights into the ultrapotassic volcanism of central Italy. Lithos 59:1–24. https://doi.org/10.1016/S0024-4937(01)00054-8

Bianchi I, Agostinetti NP, Gori PD et al (2008) Deep structure of the Colli Albani volcanic district (central Italy) from receiver functions analysis. J Geophys Res 113:B09313. https://doi.org/10.1029/2007JB005548

Blythe LS, Deegan FM, Freda C et al (2015) Co_2 bubble generation and migration during magma-carbonate interaction. Contrib Mineral Petrol 169:1–16. https://doi.org/10.1007/s00410-015-1137-4

Boari E, Avanzinelli R, Melluso L et al (2009) Isotope geochemistry (Sr-Nd-Pb) and petrogenesis of leucite-bearing volcanic rocks from "Colli Albani'' volcano, roman magmatic province, central Italy: inferences on volcano evolution and magma genesis. Bull Volcanol 71:977–1005. https://doi.org/10.1007/s00445-009-0278-6

Brehm SK, Lange RA (2020) Evidence of rapid phenocryst growth of olivine during ascent in basalts from the big pine volcanic field: application of olivine-melt thermometry and hygrometry at the liquidus. Geochem Geophys Geosyst 21(10):e2020GC009264

Calabró L, Ongaro TE, Giordano G et al (2022) Reconstructing pyroclastic currents' source and flow parameters from deposit characteristics and numerical modeling: the Pozzolane Rosse ignimbrite case study (Colli Albani, Italy). J Geophys Res Solid Earth 127. https://doi.org/10.1029/2021JB023637

Campagnola S (2015) Large scale Plinian eruptions of the Colli Albani and the Campi Flegrei volcanoes: insights from textural and rheological studies. Plinius

Campagnola S, Vona A, Romano C et al (2016) Crystallization kinetics and rheology of leucite-bearing tephriphonolite magmas from the Colli Albani volcano (Italy). Chem Geol 424:12–29. https://doi.org/10.1016/j.chemgeo.2016.01.012

Caricchi L, Annen C, Blundy J et al (2014) Frequency and magnitude of volcanic eruptions controlled by magma injection and buoyancy. Nat Geosci 7:126–130. https://doi.org/10.1038/ngeo2041

Caricchi L, Sheldrake TE, Blundy J (2018) Modulation of magmatic processes by CO_2 flushing. Earth Planet Sci Lett 491:160–171. https://www.linkinghub.elsevier.com/retrieve/pii/S0012821X18301742

Caricchi L, Townsend M, Rivalta E et al (2021) The build-up and triggers of volcanic eruptions. Nat Rev Earth Environ 2(7):458–476

Caro G, Bourdon B (2010) Non-chondritic Sm/Nd ratio in the terrestrial planets: consequences for the geochemical evolution of the mantle-crust system. Geochim Cosmochim Acta 74:3333–3349. https://doi.org/10.1016/j.gca.2010.02.025

Carrasquero SI, Rubinstein NA, Gómez AL et al (2018) New insights into petrogenesis of Miocene magmatism associated with porphyry copper deposits of the Andean Pampean flat slab. Argentina. Geosci Front 9(5):1565–1576

Cassidy M, Manga M, Cashman K et al (2018) Controls on explosive-effusive volcanic eruption styles. Nat Commun 9:1–16. https://doi.org/10.1038/s41467-018-05293-3

Chiarabba C, Amato A, Delaney PT (1997) Crustal structure, evolution, and volcanic unrest of the Alban Hills, central Italy. Bull Volcanol 59:161–170. https://doi.org/10.1007/s004450050183.

Chiaradia M, Müntener O, Beate B (2020) Effects of aseismic ridge subduction on the geochemistry of frontal arc magmas. Earth Planet Sci Lett 531:115984

Chiodini G, Cardellini C, Amato A et al (2004) Carbon dioxide earth degassing and seismogenesis in central and southern Italy. Geophys Res Lett 31:2–5. https://doi.org/10.1029/2004GL019480

Conticelli S (1998) The effect of crustal contamination on ultrapotassic magmas with Lamproitic affinity: mineralogical, geochemical and isotope data from the Torre Alfina lavas and xenoliths, central Italy. Chem Geol 149:51–81. https://doi.org/10.1016/S0009-2541(98)00038-2

Conticelli S, Antonio MD, Pinarelli L et al (2002) Source contamination and mantle heterogeneity in the genesis of Italian potassic and ultrapotassic volcanic rocks?: Sr ± nd ± Pb isotope data from roman province and southern Tuscany. Mineral Petrol 74:189–222. https://doi.org/10.1007/s007100200004

Conticelli S, Carlson RW, Widom E et al (2007) Chemical and isotopic composition (Os, Pb, Nd, and Sr) of neogene to quaternary calc-alkalic, shoshonitic, and ultrapotassic mafic rocks from the Italian peninsula: inferences on the nature of their mantle sources. Spec Pap Geol Soc Am 418:171–202. https://doi.org/10.1130/2007.2418(09)

Conticelli S, Guarnieri L, Farinelli A et al (2009) Trace elements and Sr-Nd-Pb isotopes of k-rich, shoshonitic, and calc-alkaline magmatism of the western Mediterranean region: genesis of ultrapotassic to calc-alkaline magmatic associations in a post-collisional geodynamic setting. Lithos 107:68–92. https://doi.org/10.1016/j.lithos.2008.07.016. (read Feb 8th 2022)

Conticelli S, Boari E, Avanzinelli R (2010) The Colli Albani volcano: special publications of IAVCEI. IAVCEI. https://doi.org/10.1144/IAVCEI003

Conticelli S, Avanzinelli R, Ammannati E et al (2015) The role of carbon from recycled sediments in the origin of ultrapotassic igneous rocks in the central Mediterranean. Lithos 232:174–196. https://doi.org/10.1016/j.lithos.2015.07.002

Costantini L, Bonadonna C, Houghton B et al (2009) New physical characterization of the Fontana lapilli basaltic Plinian eruption, Nicaragua. Bull Volcanol 71:337–355

Cross JK, Tomlinson EL, Giordano G et al (2014) High level triggers for explosive mafic volcanism: Albano maar, Italy. Lithos 190–191:137–153. https://doi.org/10.1016/j.lithos.2013.11.001

Dallai L, Freda C, Gaeta M (2004) Oxygen isotope geochemistry of pyroclastic clinopyroxene monitors carbonate contributions to roman-type ultrapotassic magmas. Contrib Mineral Petrol 148:247–263. https://doi.org/10.1007/s00410-004-0602-2

Degruyter W, Huber C, Bachmann O et al (2016) Magma reservoir response to transient recharge events: the case of Santorini volcano (Greece). Geology 44(1):23–26

DePaolo DJ (1981) Trace element and isotopic effects of combined wallrock assimilation and fractional crystallization. Earth Planet Sci Lett 53:189–202. https://doi.org/10.1016/0012-821X(81)90153-9

Diano G, Bonamico A, Giordano G et al (2010) Three-dimensional reconstruction of the main unconformities of the Colli Albani stratigraphy and deposit volume calculations. Spec Publ IAVCEI 3:177–188. https://doi.org/10.1144/IAVCEI003.9

Druitt TH, Costa F, Deloule E et al (2012) Decadal to monthly timescales of magma transfer and reservoir growth at a caldera volcano. Nature 482(7383):77–80

Fabbro G, Druitt TH, Scaillet S (2013) Evolution of the crustal magma plumbing system during the build-up to the 22-ka caldera-forming eruption of Santorini (Greece). Bull Volcanol 75:1–22

Federico M, Peccerillo A, Barbieri M et al (1994) Mineralogical and geochemical study of gransular xenoliths from Alban Hills Colcano, central Italy: bearing on evolutionary processes in potassic magma chambers. Contrib Mineral Petrol 115:384–401. https://doi.org/10.1007/BF00320973

Ferguson DJ, Gonnermann HM, Ruprecht P et al (2016) Magma decompression rates during explosive eruptions of Kīlauea volcano, Hawaii, recorded by melt embayments. Bull Volcanol 78:71. https://doi.org/10.1007/s00445-016-1064-x

Floess D, Baumgartner LP, Vonlanthen P (2015) An observational and thermodynamic investigation of carbonate partial melting. Earth Planet Sci Lett 409:147–156. https://doi.org/10.1016/j.epsl.2014.10.031

Freda C, Gaeta M, Palladino DM et al (1997) The Villa Senni eruption (Alban Hills, central Italy): the role of H_2O and CO_2 on the magma chamber evolution and on the eruptive scenario. J Volcanol Geotherm Res 78:103–120. https://doi.org/10.1016/S0377-0273(97)00007-3

Freda C, Gaeta M, Misiti V et al (2008) Magma-carbonate interaction: an experimental study on ultrapotassic rocks from Alban Hills (central Italy). Lithos 101:397–415. https://doi.org/10.1016/j.lithos.2007.08.008

Freda C, Gaeta M, Giaccio B et al (2011) CO_2-driven large mafic explosive eruptions: the Pozzolane Rosse case study from the Colli Albani volcanic district (Italy). Bull Volcanol 73:241–256. https://doi.org/10.1007/s00445-010-0406-3

Gaeta M, Freda C, Christensen JN et al (2006) Time-dependent geochemistry of clinopyroxene from the Alban Hills (central Italy): clues to the source and evolution of ultrapotassic magmas. Lithos 86:330–346. https://doi.org/10.1016/j.lithos.2005.05.010

Gaeta M, Freda C, Marra F et al (2016) Paleozoic metasomatism at the origin of Mediterranean ultrapotassic magmas: constraints from time-dependent geochemistry of Colli Albani volcanic products (central Italy). Lithos 244:151–164. https://doi.org/10.1016/j.lithos.2015.11.034

Gagnevin D, Daly JS, Poli G (2004) Petrographic, geochemical and isotopic constraints on magma dynamics and mixing in the Miocene Monte Capanne monzogranite (Elba Island, Italy). Lithos 78:157–195. https://doi.org/10.1016/j.lithos.2004.04.043

Geyer A, Folch A, Martí J (2006) Relationship between caldera collapse and magma chamber withdrawal: an experimental approach. J Volcanol Geotherm Res 157(4):375–386

Ghiorso MS, Sack RO (1995) Chemical mass transfer in magmatic processes iv. a revised and internally consistent thermodynamic model for the interpolation and extrapolation of liquid-solid equilibria in magmatic systems at elevated temperatures and pressures. Contrib Mineral Petrol 119:197–212. https://doi.org/10.1007/BF00307281

Giordano G, the CARG Team tCT (2010) The Colli Albani volcano. Spec Publ IAVCEI 3:43–97. https://doi.org/10.1144/IAVCEI003

Giordano G, Caricchi L (2022) Determining the state of activity of transcrustal magmatic systems and their volcanoes. Annu Rev Earth Planet Sci 50. https://doi.org/10.1146/annurev-earth-032320-084733

Giordano G, Cas RA (2021) Classification of ignimbrites and their eruptions. Earth Sci Rev 220:103697. https://doi.org/10.1016/j.earscirev.2021.103697

Giordano D, Dingwell D (2003) Viscosity of hydrous Etna basalt: implications for Plinian-style basaltic eruptions. Bull Volcanol 65:8–14. https://doi.org/10.1007/s00445-002-0233-2

Giordano D, Russell JK, Dingwell DB (2008) Viscosity of magmatic liquids: a model. Earth Planet Sci Lett 271:123–134. https://doi.org/10.1016/j.epsl.2008.03.038

Gonnermann HM, Manga M (2007) The fluid mechanics inside a volcano. Annu Rev Fluid Mech 39(1):321–356. https://doi.org/10.1146/annurev.fluid.39.050905.110207

Gualda GAR, Ghiorso MS (2015) Melts.excel: a microsoft excel based melts interface for research and teaching of magma properties and evolution. Geochem Geophys Geosyst 16:315–324. https://doi.org/10.1002/2014GC005545

Hamilton DL, Burnham CW, Osborn EF (1964) The solubility of water and effects of oxygen fugacity and water content on crystallization in mafic magmas. J Petrol 5:21–39. https://doi.org/10.1093/petrology/5.1.21

Higgins O, Caricchi L (2023) Eruptive dynamics reflect crustal structure and mantle productivity beneath volcanoes. Geology. https://doi.org/10.1130/G51355.1

Hirschmann MM, Ghiorso MS, Davis FA et al (2008) Library of experimental phase relations (LEPR): a database and web portal for experimental magmatic phase equilibria data. Geochem Geophys Geosyst 9. https://doi.org/10.1029/2007GC001894

Hlinka L, Longpré MA, Pérez W et al (2021) Top-down control on eruptive style at Masaya volcano inferred from melt composition. Earth Planet Sci Lett 572:117138

Huber C, Su Y, Nguyen C et al (2014) A new bubble dynamics model to study bubble growth, deformation, and coalescence. J Geophys Res Solid Earth 119(1):216–239

Iacono-Marziano G, Gaillard F, Pichavant M (2007) Limestone assimilation and the origin of CO_2 emissions at the Alban Hills (central Italy): constraints from experimental petrology. J Volcanol Geotherm Res 166:91–105. https://doi.org/10.1016/j.jvolgeores.2007.07.001

Iacono-Marziano G, Gaillard F, Pichavant M (2008) Limestone assimilation by basaltic magmas: an experimental re-assessment and application to Italian volcanoes. Contrib Mineral Petrol 155:719–738. https://doi.org/10.1007/s00410-007-0267-8

Jaeger JC (1965) Application of the theory of heat conduction to geothermal measurements. American Geophysical Union, Washington D.C. https://doi.org/10.1029/GM008p0007

Jellinek AM, DePaolo DJ (2003) A model for the origin of large silicic magma chambers: precursors of caldera-forming eruptions. Bull Volcanol 65:363–381

Jorgenson C, Higgins O, Petrelli M et al (2022) A machine learning-based approach to clinopyroxene thermobarometry: model optimization and distribution for use in earth sciences. J Geophys Res Solid Earth 127. https://doi.org/10.1029/2021JB022904

Karner DB, Marra F, Renne PR (2001) The history of the Monti Sabatini and Alban Hills volcanoes: ground for assessing volcanic-tectonic hazards for Rome. J Volcanol Geotherm Res 107:185–219. https://doi.org/10.1016/S0377-0273(00)00258-4

Knuever M, Sulpizio R, Mele D et al (2022) Magma-rock interactions: a review of their influence on magma rising processes with emphasis on short-timescale assimilation of carbonate rocks. Geol Soc Lond Spec Publ. https://doi.org/10.1144/sp520-2021-177

Lustrino M, Ronca S, Caracausi A et al (2020) Strongly SiO_2 -undersaturated, CaO-rich Kamafugitic Pleistocene magmatism in central Italy (San Venanzo volcanic complex) and the role of shallow depth limestone assimilation. Earth Sci Rev 208:103256. https://doi.org/10.1016/j.earscirev.2020.103256

MacDonald DUD (2017) Data reduction guide-understanding EPMA analytical results. https://www.dal.ca/sites/electron-microprobe-lab/analysis/drg_9.html. Last accessed 09-11-2023

Marshall AA, Brand BD, Martínez V et al (2022) The mafic Curacautín ignimbrite of Llaima volcano. Chile. J Volcanol Geotherm Res 421:107418

Masotta M, Mollo S, Freda C et al (2013) Clinopyroxene-liquid thermometers and barometers specific to alkaline differentiated magmas. Contrib Mineral Petrol 166:1545–1561. https://doi.org/10.1007/s00410-013-0927-9

McArthur JM, Howarth R, Bailey T (2001) Strontium isotope stratigraphy: LOWESS version 3: best fit to the marine Sr-isotope curve for 0–509 Ma and accompanying look-up table for deriving numerical age. J Geol 109(2):155–170

Melluso L, Conticelli S, D'Antonio M et al (2004) Petrology and mineralogy of Wollastonite- and melilite-bearing Paralavas from the central Apennines, Italy. Am Mineral 88:1287–1299. https://doi.org/10.2138/am-2003-8-911

Metrich N, Bertagnini A, Landi P et al (2001) Crystallization driven by decompression and water loss at Stromboli volcano (Aeolian Islands, Italy). J Petrol 42:1471–1490. https://doi.org/10.1093/petrology/42.8.1471

Mollo S, Gaeta M, Freda C et al (2010) Carbonate assimilation in magmas: a reappraisal based on experimental petrology. Lithos 114:503–514. https://doi.org/10.1016/j.lithos.2009.10.013

Moussallam Y, Morizet Y, Massuyeau M et al (2015) CO_2 solubility in kimberlite melts. Chem Geol 418:198–205. https://doi.org/10.1016/j.chemgeo.2014.11.017

Neave DA, Putirka KD (2017) A new clinopyroxene-liquid barometer, and implications for magma storage pressures under icelandic rift zones. Am Mineral 102:777–794. https://doi.org/10.2138/am-2017-5968

Neave DA, Namur O, Shorttle O et al (2019) Magmatic evolution biases basaltic records of mantle chemistry towards melts from recycled sources. Earth Planet Sci Lett 520:199–211. https://doi.org/10.1016/j.epsl.2019.06.003

Ohashi M, Maruishi T, Toramaru A (2022) Coalescence of growing bubbles in highly viscous liquids. Geochem Geophys Geosyst 23(11):e2022GC010618

Palladino DM, Gaeta M, Marra F (2001) A large K-foiditic hydromagmatic eruption from the early activity of the Alban Hills Volcanic District. Italy. Bull Volcanol 63(5):345–359. https://doi.org/10.1007/s004450100150

Pallister JS, Hoblitt RP, Reyes AG (1992) A basalt trigger for the 1991 eruptions of Pinatubo volcano? Nature 356(6368):426–428

Papale P, Neri A, Macedonio G (1999) The role of water content and magma composition on explosive eruption dynamics. Phys Chem Earth Part A Solid Earth Geod 24:969–975. https://doi.org/10.1016/S1464-1895(99)00144-1

Petrelli M, Caricchi L, Perugini D (2020) Machine learning thermo 'barometry: application to clinopyroxene' bearing magmas. J Geophys Res Solid Earth 125. https://doi.org/10.1029/2020JB020130

Pin C, Briot D, Bassin C et al (1994) Concomitant separation of strontium and samarium-neodymium for isotopic analysis in silicate samples, based on specific extraction chromatography. Anal Chim Acta 298(2):209–217

Plank T, Kelley KA, Zimmer MM et al (2013) Why do mafic arc magmas contain 4 wt% water on average? Earth Planet Sci Lett 364:168–179. https://doi.org/10.1016/j.epsl.2012.11.044

Putirka KD (2008) Thermometers and barometers for volcanic systems. Rev Mineral Geochem 69:61–120. https://doi.org/10.2138/rmg.2008.69.3

Roggensack K, Hervig RL, McKnight SB et al (1997) Explosive basaltic volcanism from Cerro Negro volcano: influence of volatiles on eruptive style. Science 277(5332):1639–1642

Rowe MC, Carey RJ, White JD et al (2021) Tarawera 1886: an integrated review of volcanological and geochemical characteristics of a complex basaltic eruption. N Z J Geol Geophys 64(2–3):296–319

Sable JE, Houghton BF, Carlo PD et al (2006) Changing conditions of magma ascent and fragmentation during the Etna 122 bc basaltic Plinian eruption: evidence from clast microtextures. J Volcanol Geotherm Res 158:333–354. https://doi.org/10.1016/j.jvolgeores.2006.07.006

Salters VJ, Stracke A (2004) Composition of the depleted mantle. Geochem Geophys Geosyst 5. https://doi.org/10.1029/2003GC000597

Shaw CSJ (2018) Evidence for the presence of carbonate melt during the formation of cumulates in the Colli Albani volcanic district, Italy. Lithos 310–311:105–119. https://doi.org/10.1016/j.lithos.2018.04.007

Sparks RS (2003) Dynamics of magma degassing. Geol Soc Lond Spec Publ 213(1):5–22. https://doi.org/10.1144/GSL.SP.2003.213.01.02

Stoppa F, Rosatelli G (2009) Ultramafic intrusion triggers hydrothermal explosions at Colle Fabbri (Spoleto, Umbria), Italy. J Volcanol Geotherm Res 187:85–92. https://doi.org/10.1016/j.jvolgeores.2009.08.013

Streck MJ (2008) Mineral textures and zoning as evidence for open system processes. Rev Mineral Geochem 69(1983):595–622. https://doi.org/10.2138/rmg.2008.69.15

Tanaka T, Togashi S, Kamioka H et al (2000) JNDI-1: a neodymium isotopic reference in consistency with Lajolla neodymium. Chem Geol 168(3–4):279–281

Tomiya A, Takahashi E (2005) Evolution of the magma chamber beneath Usu volcano since 1663: a natural laboratory for observing changing phenocryst compositions and textures. J Petrol 46(12):2395–2426. https://doi.org/10.1093/petrology/egi057

Trasatti E, Marra F, Polcari M et al (2018) Coeval uplift and subsidence reveal magma recharging near Rome (Italy). Geochemi Geophys Geosyst 19. https://doi.org/10.1029/2017GC007303

Trolese M, Giordano G, Cifelli F et al (2017) Forced transport of thermal energy in magmatic and phreatomagmatic large volume ignimbrites: paleomagnetic evidence from the Colli Albani volcano, Italy. Earth Planet Sci Lett 478:179–191. https://doi.org/10.1016/j.epsl.2017.09.004

Ubide T, Mollo S, Jx Zhao et al (2019) Sector-zoned clinopyroxene as a recorder of magma history, eruption triggers, and ascent rates. Geochim Cosmochim Acta 251:265–283. https://doi.org/10.1016/j.gca.2019.02.021

Vetere F, Holtz F, Behrens H et al (2014) The effect of alkalis and polymerization on the solubility of H_2O and CO_2 in alkali-rich silicate melts. Contrib Mineral Petrol 167:1–17

Vinkler AP, Cashman K, Giordano G et al (2012) Evolution of the mafic Villa Senni caldera-forming eruption at Colli Albani volcano, Italy, indicated by textural analysis of juvenile fragments. J Volcanol Geotherm Res 235–236:37–54. https://doi.org/10.1016/j.jvolgeores.2012.03.006

Wang X, Hou T, Wang M et al (2021) A new clinopyroxene thermobarometer for mafic to intermediate magmatic systems. Eur J Mineral 33(5):621–637

Welsch B, Hammer J, Baronnet A et al (2016) Clinopyroxene in post-shield Haleakala ankaramite: 2. Texture, compositional zoning and supersaturation in the magma. Contrib Mineral Petrol 171(6). https://doi.org/10.1007/s00410-015-1213-9

Whittington AG, Hofmeister AM, Nabelek PI (2009) Temperature-dependent thermal diffusivity of the earth's crust and implications for magmatism. Nature 458:319–321. https://doi.org/10.1038/nature07818

Wyllie PJ, Tuttle F (1960) The system CaO-CO_2-H_2O and the origin of carbonatites. J Petrol 1:1–46. https://doi.org/10.1093/petrology/1.1.1